Published for SISSA by Springer

Received: *March 6, 2015*
Revised: *May 1, 2015*
Accepted: *May 19, 2015*
Published: *June 12, 2015*

Search for vector-like T quarks decaying to top quarks and Higgs bosons in the all-hadronic channel using jet substructure

The CMS collaboration

E-mail: cms-publication-committee-chair@cern.ch

Abstract: A search is performed for a vector-like heavy T quark that is produced in pairs and that decays to a top quark and a Higgs boson. The data analysed correspond to an integrated luminosity of $19.7\,\mathrm{fb}^{-1}$ collected with the CMS detector in proton-proton collisions at $\sqrt{s} = 8\,\mathrm{TeV}$. For T quarks with large mass values the top quarks and Higgs bosons can have significant Lorentz boosts, so that their individual decay products often overlap and merge. Methods are applied to resolve the substructure of such merged jets. Upper limits on the production cross section of a T quark with mass between 500 and $1000\,\mathrm{GeV}/c^2$ are derived. If the T quark decays exclusively to tH, the observed (expected) lower limit on the mass of the T quark is 745 (773) GeV/c^2 at 95% confidence level. For the first time an algorithm is used for tagging boosted Higgs bosons that is based on a combination of jet substructure information and b tagging.

Keywords: Hadron-Hadron Scattering, Beyond Standard Model, Top physics

ArXiv ePrint: 1503.01952

doi:10.1007/JHEP06(2015)080

JHEP06(2015)080

Contents

1 Introduction

The discovery of a Higgs boson with a mass of 125 GeV/c^2 [1, 2] motivates the search for exotic states involving the newly discovered particle. The mechanism that stabilizes the mass of the Higgs particle is not entirely clear and could be explained by little Higgs models [3, 4], models with extra dimensions [5, 6], and composite Higgs models [5–7]. These theories predict the existence of heavy vector-like quarks that may decay into top quarks and Higgs bosons. This article presents a search for exotic resonances decaying into Higgs bosons and top quarks. A model of vector-like T quarks with charge $2/3\,e$, which are produced in pairs by the strong interaction, is used as a benchmark for this analysis.

The left-handed and right-handed components of vector-like quarks transform in the same way under the standard model (SM) symmetry group $\mathrm{SU}(3)_c \times \mathrm{SU}(2)_L \times \mathrm{U}(1)_Y$. This allows direct mass terms in the Lagrangian of the form $m\overline{\psi}\psi$ that do not violate gauge invariance. As a consequence, vector-like quarks do not acquire their mass via Yukawa couplings, in contrast to the other quark families. A fourth generation of chiral fermions, replicating one of the three generations of the SM with identical quantum numbers, is disfavoured by electroweak fits within the framework of the SM [8]. This is because of the large modifications to the Higgs production cross sections and branching fractions, if a single SM-like Higgs doublet is assumed. Vector-like heavy quarks are not similarly constrained by the measurements of the Higgs boson properties [9].

Vector-like T quarks can decay into three different final states: tH, tZ, and bW [9]. The assumption of decays with 100% branching fraction ($\mathcal{B}$) has been used in various searches by the ATLAS and CMS collaborations [10–13]. Other searches that do not make specific assumptions on the branching fractions have also been performed [14]. In the present analysis the event selection is optimized to be sensitive to exclusive T quark decays to tH. In addition, the results are quoted as a function of the branching fractions to the three decay modes: tH, tZ, and bW.

While searches for T quarks have been performed in leptonic final states [10–14], this article presents the first analysis that exploits the all-hadronic final state in the search for vector-like quarks. In the SM the Higgs boson decays predominantly into b quark pairs with a branching fraction of 58% for a mass of $125\,\mathrm{GeV}/c^2$, while the top quark decays almost exclusively into a bottom quark and a W boson, which in turn decays hadronically 67.6% of the time. The main final state is therefore the all-hadronic final state $\mathrm{T} \to \mathrm{tH} \to (\mathrm{b}jj)(\mathrm{b\overline{b}})$, where j denotes the light-flavour jets of the W boson decay and b denotes the b-flavour jets from the top quark or Higgs boson decays. For sufficiently large T quark mass values, the decay products can be highly Lorentz-boosted, leading to final states with overlapping and merged jets. In the extreme case, all top quark decay products are merged into a single jet. A similar topology may arise for the Higgs boson decaying into b quarks. A related analysis concept has been proposed in ref. [15]. In recent years, the methodology of jet substructure analysis has proved to be very powerful in resolving such boosted topologies [16–19]. For example, the analysis of high-mass Z' resonances decaying into top quark pairs became feasible in the all-hadronic final state as a result of the application of jet substructure methods [20–22]. A similar strategy is followed in this analysis by applying algorithms for the identification of boosted top quarks (t tagging) and boosted Higgs bosons (H tagging) in combination with algorithms for the identification of b quark jets (b tagging). In particular, the application of b tagging in subjets has enhanced the identification of boosted $\mathrm{b\overline{b}}$ final states, for instance $\mathrm{H} \to \mathrm{b\overline{b}}$ decays. This is the first analysis to apply an algorithm for tagging boosted Higgs bosons that is based on a combination of jet substructure information and b tagging.

2 The CMS detector

The central feature of the CMS apparatus is a superconducting solenoid of 6 m internal diameter. Within the superconducting solenoid volume are a silicon pixel and strip tracker,

JHEP06(2015)080

a lead tungstate crystal electromagnetic calorimeter (ECAL), and a brass and scintillator hadron calorimeter (HCAL), each composed of a barrel and two endcap sections. Muons are measured in gas-ionization detectors embedded in the steel flux-return yoke outside the solenoid. Extensive forward calorimetry complements the coverage provided by the barrel and endcap detectors.

The energy resolution for photons with $E_{\mathrm{T}} \approx 60\,\mathrm{GeV}$ varies between 1.1 and 2.6% over the solid angle of the ECAL barrel, and from 2.2 to 5% in the endcaps. The HCAL, when combined with the ECAL, measures jets with a resolution $\Delta E/E \approx 100\%/\sqrt{E\,[\mathrm{GeV}]} \oplus 5\%$ [23].

In the region $|\eta| < 1.74$, the HCAL cells have widths of 0.087 in η and 0.087 in azimuth (ϕ). In the η-ϕ plane, and for $|\eta| < 1.48$, the HCAL cells map on to 5×5 ECAL crystal arrays to form calorimeter towers projecting radially outwards from close to the nominal interaction point. At larger values of $|\eta|$, the size of the towers increases and the matching ECAL arrays contain fewer crystals. Within each tower, the energy deposits in ECAL and HCAL cells are summed to define the calorimeter tower energies, subsequently used to provide the energies and directions of hadronic jets.

The silicon tracker measures charged particles within the pseudorapidity range $|\eta| < 2.5$. It consists of 1440 silicon pixel and 15 148 silicon strip detector modules and is located in the 3.8 T field of the superconducting solenoid. For nonisolated particles of $1 < p_{\mathrm{T}} < 10\,\mathrm{GeV}/c$ and $|\eta| < 1.4$, the track resolutions are typically 1.5% in p_{T} and 25–90 (45–150) μm in the transverse (longitudinal) impact parameter [24].

A more detailed description of the CMS detector, together with a definition of the coordinate system used and the relevant kinematic variables, can be found in ref. [25].

3 Event samples

The data used for this analysis were collected by the CMS experiment using pp collisions provided by the CERN LHC with a centre-of-mass energy of 8 TeV, and correspond to an integrated luminosity of $19.7\,\mathrm{fb}^{-1}$. Events are selected online by a trigger algorithm that requires H_{T}, the scalar sum of the transverse momenta of reconstructed jets in the detector, to be greater than $750\,\mathrm{GeV}/c$. The online H_{T} is calculated from calorimeter jets with $p_{\mathrm{T}} > 40\,\mathrm{GeV}/c$. Calorimeter jets are reconstructed from the energy deposits in the calorimeter towers, clustered by the anti-k_{T} algorithm [26, 27] with a size parameter of 0.5.

Simulated samples are used to determine signal selection efficiencies as well as the background contribution from $\mathrm{t\bar{t}}$ plus jets, $\mathrm{t\bar{t}}H$, and hadronically decaying W/Z plus b jet production. The background from QCD multijet production is derived from data.

Events from T quark decays are generated for mass hypotheses between 500 and $1000\,\mathrm{GeV}/c^2$ in steps of $100\,\mathrm{GeV}/c^2$. The inclusive cross sections for the signal samples and $\mathrm{t\bar{t}}$ samples are calculated at next-to-next-to-leading order (NNLO) for the reaction $\mathrm{gg} \to \mathrm{t\bar{t}} + X$. The fixed order calculations are supplemented with soft-gluon resummation with next-to-next-to-leading logarithmic accuracy [28]. The $\mathrm{t\bar{t}}$ cross sections are computed based on the Top++ v2.0 implementation using the MSTW2008nnlo68cl parton distribution functions (PDF) and the 5.9.0 version of LHAPDF [28, 29]. The evaluated

$t\bar{t}$ cross section is 252.9 pb, assuming a top quark mass of 172.5 GeV/c^2. The theoretical pair-production cross sections for the signal samples are listed in table 1.

The mass of the Higgs boson in the signal samples is set to 120 GeV/c^2, as the samples were produced before the discovery of the Higgs boson. The branching fractions of the Higgs boson decays are corrected to the expected values for a Higgs boson with a mass of 125 GeV/c^2 using the recommendations from ref. [30]. The difference between the actual mass of the Higgs boson (125 GeV/c^2) and the simulated mass (120 GeV/c^2) has no impact on the analysis results.

The $t\bar{t}$ background sample is generated with POWHEG v1.0 [31–33] interfaced to PYTHIA 6.426 [34] to simulate the parton shower and hadronisation. All other background samples and the signal samples are simulated with MADGRAPH 5.1 [35], interfaced with PYTHIA 6.426. The CTEQ6L1 [36] PDF set is used with MADGRAPH, while the POWHEG samples have been produced with CTEQ6M. For PYTHIA, the Z2* tune is used to simulate the underlying event [37].

Simulated QCD multijet samples are used to validate the estimation of this background from data. These samples are simulated with MADGRAPH in the same way as the other background samples described above.

4 Event reconstruction

Tracks are reconstructed using an iterative tracking procedure [24]. The primary vertices are reconstructed with a deterministic annealing method [38] from all tracks in the event that are compatible with the location of the proton-proton interaction region. The vertex with the highest $\sum(p_{\mathrm{T}}^{\mathrm{track}})^2$ is defined as the primary interaction vertex, whose position is determined from an adaptive vertex fit [39].

The particle-flow event algorithm [40, 41] reconstructs and identifies each individual particle with an optimized combination of information from the various elements of the CMS detector. The energy of photons is directly obtained from the ECAL measurement, corrected for zero-suppression effects. The energy of electrons is determined from a combination of the electron momentum at the primary interaction vertex as determined by the tracker, the energy of the corresponding ECAL cluster, and the energy sum of all bremsstrahlung photons spatially compatible with originating from the electron track. The energy of muons is obtained from the curvature of the corresponding track. The energy of charged hadrons is determined from a combination of their momentum measured in the tracker and the matching ECAL and HCAL energy deposits, corrected for zero-suppression effects and for the response function of the calorimeters to hadronic showers. Finally, the energy of neutral hadrons is obtained from the corresponding corrected ECAL and HCAL energy.

For each event, hadronic jets are clustered from these reconstructed particles with the infrared and collinear-safe anti-k_{t} algorithm or with the Cambridge-Aachen algorithm (CA jets) [42]. The jet momentum is defined to be the vector sum of all particle momenta in this jet, and is found in the simulation to be within 5% to 10% of the true momentum over the whole p_{T} spectrum and detector acceptance. Jet energy corrections are derived from the simulation, and are confirmed with in situ measurements using the energy balance of dijet and photon+jet events [43]. The jet energy resolution amounts typically to 15% at 10 GeV, 8% at 100 GeV, and 4% at 1 TeV, to be compared to about 40%, 12%, and 5% obtained when the calorimeters are used alone for jet clustering.

The jets contain neutral particles from additional collisions within the same beam crossing (pileup). The contribution from these additional particles is subtracted based on the average expectation of the energy deposited from pileup in the jet area, using the methods described in ref. [44].

For the identification of b jets, the combined secondary vertex (CSV) algorithm is used and the medium operating point (CSVM) is applied [45]. With this operating point the b tagging efficiency is 70% and the light flavour jet misidentification rate is 1% in $\mathrm{t\bar{t}}$ events. This algorithm uses information from reconstructed tracks and secondary vertices that are displaced from the primary interaction vertex. The information is combined into a single discriminating variable. The same b tagging algorithm is used in boosted topologies and the corresponding efficiencies and misidentification rates are tested in the relevant samples. More details on b tagging in boosted topologies are given in section 6.

5 Analysis strategy

Event selection criteria that make use of novel jet substructure methods are applied to reduce the large background contributions from QCD multijet and $\mathrm{t\bar{t}}$ events in the analysis. The jet substructure methods are described in detail in section 6 and the event selection criteria are summarized in section 7.

Two variables are used to distinguish signal from background events after the event selection. These variables are H_T and the invariant mass $m_{\mathrm{b\bar{b}}}$ of two b-tagged subjets in Higgs boson candidate jets. High H_T values characterize events with large hadronic activity as in the case of signal events.

The shape and normalization of the H_T and $m_{\mathrm{b\bar{b}}}$ distributions of QCD multijet events in this analysis are derived using data in signal-depleted sideband regions. The sideband regions are defined by inverting the jet substructure criteria. Closure tests are performed with simulated QCD events to verify that the method predicts the rates and shapes of H_T and $m_{\mathrm{b\bar{b}}}$ accurately. The background determination is discussed in detail in section 8.

The H_T and $m_{\mathrm{b\bar{b}}}$ variables are combined into a single discriminator that enhances the sensitivity of the analysis. This combination is performed using a likelihood ratio method, which is described in section 10.

Two event categories are used in the statistical interpretation of the results: a category with a single Higgs boson candidate and a category with at least two Higgs boson candidates. These are denoted as single and multiple H tag categories. They are chosen as such to be statistically independent and are combined in setting the final limit. For the multiple H tag category, the Higgs boson candidate with the highest transverse momentum is used in the likelihood definition. The procedure of the limit setting is discussed in detail in section 10.

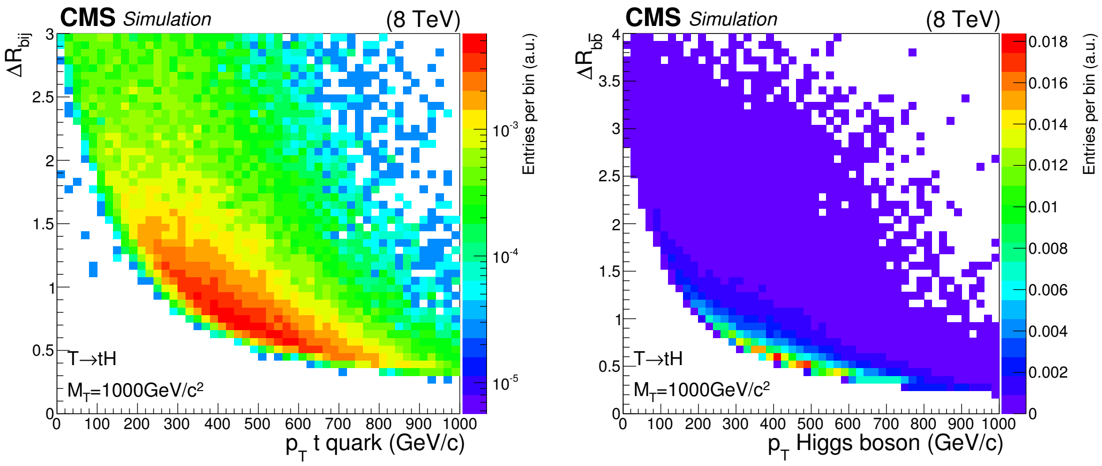

Figure 1. The distribution of the angular distance $\Delta R_{\mathrm{b}ij}$ between the three top quark decay products as a function of the top quark p_{T} for simulated T quark events with a T quark mass of $1000\,\mathrm{GeV}/c^2$ (left). Distribution of the angular distance $\Delta R_{\mathrm{b\bar{b}}}$ of the two generated b quarks from Higgs boson decays versus the Higgs boson p_{T}, for the same event sample (right).

6 Jet substructure methods

Because of the large mass of the T quarks, the top quarks and Higgs bosons from T quark decays would have significant Lorentz boosts. Daughter particles of these top quarks are therefore not well separated. In many cases all of the top quark decay products are clustered into a single, large jet by the event reconstruction algorithms. The approximate spread of a hadronic top quark decay can be determined on simulated events from the ΔR distances between the quarks produced during its decay. The four-momenta of the two quarks with the smallest ΔR distance, $\Delta R(\mathrm{q}_1, \mathrm{q}_2)$, are vectorially summed and the ΔR distance between the vector sum and the third quark, $\Delta R(\mathrm{q}_{1+2}, \mathrm{q}_3)$, is evaluated. The maximum distance between $\Delta R(\mathrm{q}_1, \mathrm{q}_2)$ and $\Delta R(\mathrm{q}_{1+2}, \mathrm{q}_3)$ indicates the approximate size $\Delta R_{\mathrm{b}ij}$ needed to cluster the entire top quark decay within one single CA jet. For the boosted decays of a Higgs boson in $\mathrm{H} \to \mathrm{b\bar{b}}$ events, the corresponding quantity can be defined as the angular distance $\Delta R_{\mathrm{b\bar{b}}} = \sqrt{(\Delta\eta)^2 + (\Delta\phi)^2}$ between the two generated b quarks. Figure 1 shows the distributions of these quantities plotted as a function of the transverse momentum of the top quark and of the Higgs boson, generated from the decay of a T quark with a mass of $1000\,\mathrm{GeV}/c^2$. This shows that, for large transverse momenta, and hence for large T quark mass values, the decay products from Higgs bosons and top quarks are generally collimated and are difficult to separate using standard jet reconstruction algorithms.

The approach adopted by this analysis is to apply the CA algorithm using a large size parameter $R = 1.5$, in order to cluster the decay products from top quarks and Higgs bosons into single large CA jets, using an implementation based on FastJet 3.0 [27]. To identify these so called "top jets" and "Higgs jets", the analysis uses dedicated jet substructure tools, in particular a t tagging algorithm and a H tagging algorithm that relies on b tagging of individual subjets. A more detailed description of these algorithms is provided in the following sections.

JHEP06(2015)080

6.1 Subjet b tagging and H tagging

It is not possible to identify b jets in boosted top quark decays using the standard CMS b tagging algorithms, since these are based on separated, non-overlapping jets. For dense environments where standard jet reconstruction algorithms are not suitable, two dedicated b tagging concepts have been investigated:

- tagging of CA jets, reconstructed using a distance parameter of 0.8 (CA8 jets) or 1.5 (CA15 jets). The 0.8 and the 1.5 jet size parameters are used because they have been found to provide optimal performance for large and for intermediate boost ranges, respectively, as discussed in the following sections.
- tagging of subjets that are reconstructed within CA jets.

The subjets of CA15 jets are reconstructed using the "filtering algorithm" [16], splitting jets into subjets based on an angular distance of $R = 0.3$. Only the three highest p_{T} subjets are retained. This filtering algorithm has been found to provide the best mass resolution for CA15 jets compared to the jet pruning [46] and trimming [47] algorithms. The pruning, trimming, and filtering algorithms are often referred to as jet grooming algorithms and their main purpose is to remove soft and wide-angle radiation as well as pileup contributions. Subjets of CA8 jets are reconstructed using the pruning algorithm, which is found to give the best performance for the reduced jet size.

For the application of b tagging to CA jets, tracks in a wide region around the jet axis are considered. The association region corresponds to the size of the CA jet. For the application of b tagging to subjets, tracks in a region of $\Delta R < 0.3$ around the subjet axis are used by the b tagging algorithm. This is the cone size employed by the standard CMS b tagging algorithms, and has also been found to give good performance for subjet b tagging.

The advantage of subjet b tagging is that it allows two subjets within a single CA jet to be identified as b jets. This is the main component of the H tagging algorithm that distinguishes between boosted Higgs bosons decaying to $\mathrm{b\overline{b}}$ and boosted top quarks.

6.1.1 Algorithm performance

Figure 2 shows the performance of subjet b tagging compared to CA15 jet b tagging for events with boosted top quarks that originate from T quark decays. The choice of the clustering algorithm and the cone size is driven by the t tagging algorithm, described in section 6.2. The b tagging efficiency is plotted versus the misidentification probability for inclusive QCD jets. Two different regions of transverse jet momentum are shown. It can be seen that subjet b tagging outperforms the CA15 jet b tagging.

For the identification of boosted Higgs bosons, two subjets must be b tagged and their invariant mass must be greater than $60\,\mathrm{GeV}/c^2$. Both CA8 jets and CA15 jets are considered. The performance of the H tagging algorithm is shown in figure 3 for two different regions of transverse jet momentum. The tagging efficiency is shown versus the misidentification probability for inclusive QCD jets. Figure 4 shows the performance obtained when evaluating the misidentification probability from $\mathrm{t\overline{t}}$ events. The performance of the standard b tagging algorithm based on AK5 jets is also shown. A CA15 jet is considered

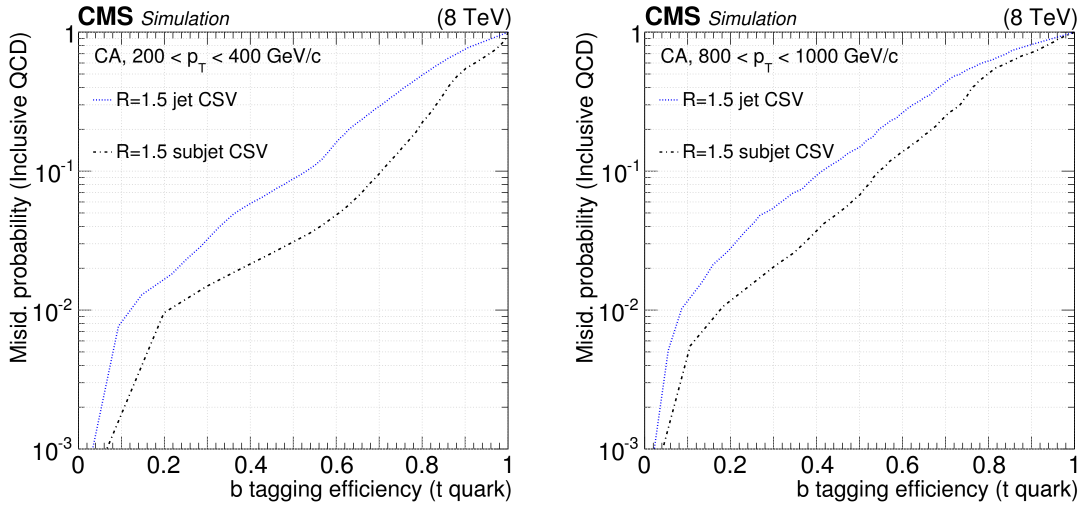

Figure 2. Performance of the CSV b tagging algorithm in simulated events with CA15 jets and with subjets within the same CA15 jet. The misidentification probability for inclusive QCD jets is shown versus the b tagging efficiency for boosted top quarks originating from T quark decays, for CA15 jet transverse momentum ranges of (left) $200 < p_{\mathrm{T}} < 400\,\mathrm{GeV}/c$ and (right) $800 < p_{\mathrm{T}} < 1000\,\mathrm{GeV}/c$.

as satisfying the H tagging requirement if two AK5 jets satisfy the b tagging requirement and have a ΔR distance <1.1 from the CA15 jet. Overall, subjet b tagging is found to provide better performance than b tagging based on AK5 jets. The choice of the optimal CA jet size parameter R depends on the p_{T} region considered. A size of $R = 1.5$ is found to be optimal for most signal mass hypotheses and is chosen for the analysis.

6.1.2 Scale factors

The subjet b tagging efficiency has been measured in data using a sample of semileptonic $\mathrm{t\bar{t}}$ events. Scale factors have been derived to correct the efficiency predicted by simulation to that measured in data. The "flavor-tag consistency" (FTC) method [45] has been used to measure these scale factors. The FTC method requires consistency between the number of b-tagged jets in data and simulation for boosted top quark events. A maximum likelihood fit is performed in which the b tagging efficiency scale factor SF_{b} and the $\mathrm{t\bar{t}}$ cross section are free parameters. Usually the light flavour misidentification scale factor SF_{light} is fixed to a value obtained independently, but in this case the simultaneous fit of SF_{light}, SF_{b}, and the $\mathrm{t\bar{t}}$ cross section has been performed for the first time. This method relies on simulation for the flavour of the subjets. A systematic uncertainty of 2% in the subjet flavour composition is taken into account.

The FTC method is applied to three different p_{T} regions of the CA15 jet: $150 \leq p_{\mathrm{T}} < 350\,\mathrm{GeV}/c$, $p_{\mathrm{T}} \geq 350\,\mathrm{GeV}/c$, and $p_{\mathrm{T}} \geq 450\,\mathrm{GeV}/c$. No significant deviation of the scale factors for the three different samples is observed. Both the scale factors SF_{b} and SF_{light} are found to be in agreement with the scale factors measured for standard b tagging of AK5 jets in the non-boosted regime.

The efficiency of the invariant mass selection requirement for the two b-tagged subjets of the Higgs boson candidate is validated with a sample of semileptonic $\mathrm{t\bar{t}}$ events. Since no

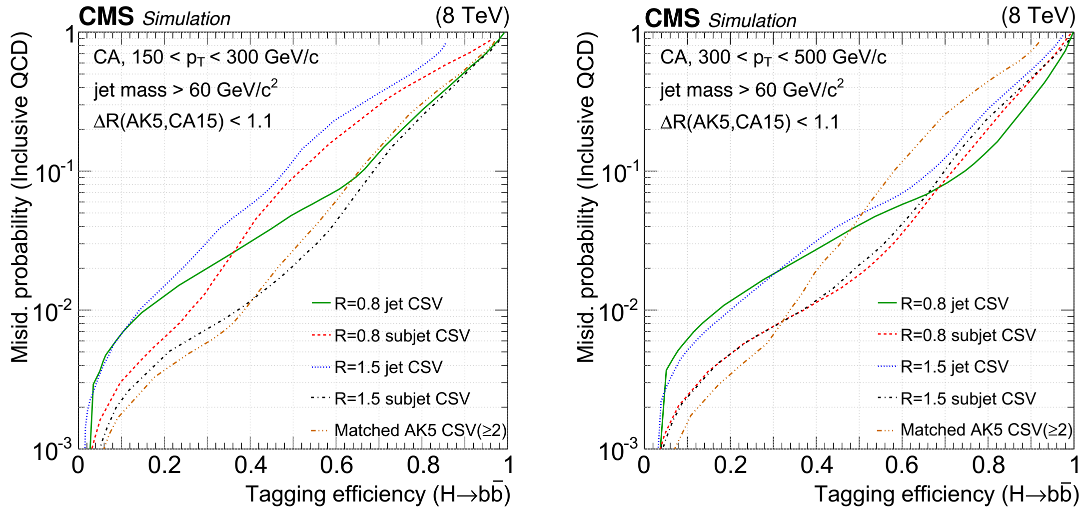

Figure 3. Performance of different H tagging algorithms in simulated signal events, with a signal mass hypothesis of $1000\,\mathrm{GeV}/c^2$. The misidentification probability for inclusive QCD jets is shown versus the tagging efficiency for boosted Higgs boson decays, for jet transverse momentum ranges of (left) $150 < p_\mathrm{T} < 300\,\mathrm{GeV}/c$ and (right) $300 < p_\mathrm{T} < 500\,\mathrm{GeV}/c$. Different b tagging options are compared: standard b tagging of AK5 jets, subjet b tagging of CA15 and CA8 jets, and b tagging of CA15 jets and CA8 jets. For the case of subjet b tagging, two subjets are required to pass the b tagging criteria. Similarly, two AK5 jets are required to pass the b tagging criteria for standard b tagging.

sample of Higgs bosons decaying into b quark pairs can be obtained in data, the validation procedure is based on the selection of a pure sample of W bosons.

The selection of semileptonic $\mathrm{t\bar{t}}$ events requires a muon and a b-tagged AK5 jet. In addition, one CA15 jet is required to be selected by the t tagging algorithm (see section 6.2). The t-tagged jet must have exactly one b-tagged subjet. The two subjets that are not b-tagged are used to calculate the invariant mass of a W boson candidate. The distribution of the W boson candidate mass is shown in figure 5. The shape of the W boson candidate mass distribution is the same in data and simulation and no additional scale factors or systematic uncertainties are assigned.

6.2 t tagging

The HEPTopTagger algorithm, described in ref. [19], is applied based on the implementation in FastJet 3.0 [27]. The algorithm uses CA15 jets as input. This choice of jet size is suitable for the region of phase space with intermediate boosts (with a jet p_T slightly above $200\,\mathrm{GeV}/c$). When the T quark mass is below $1\,\mathrm{TeV}/c^2$, a considerable fraction of the decay products populate the intermediate boost range. Such resolved events could in principle be reconstructed with standard methods using AK5 jets. The HEPTopTagger provides a seamless transition between the non-boosted and boosted domains.

For each jet, the HEPTopTagger analyses the substructure by stepping backward through the clustering history of the jet in an iterative procedure until the conditions for splitting are no longer fulfilled and the subjets are not split any further. The filtering algo-

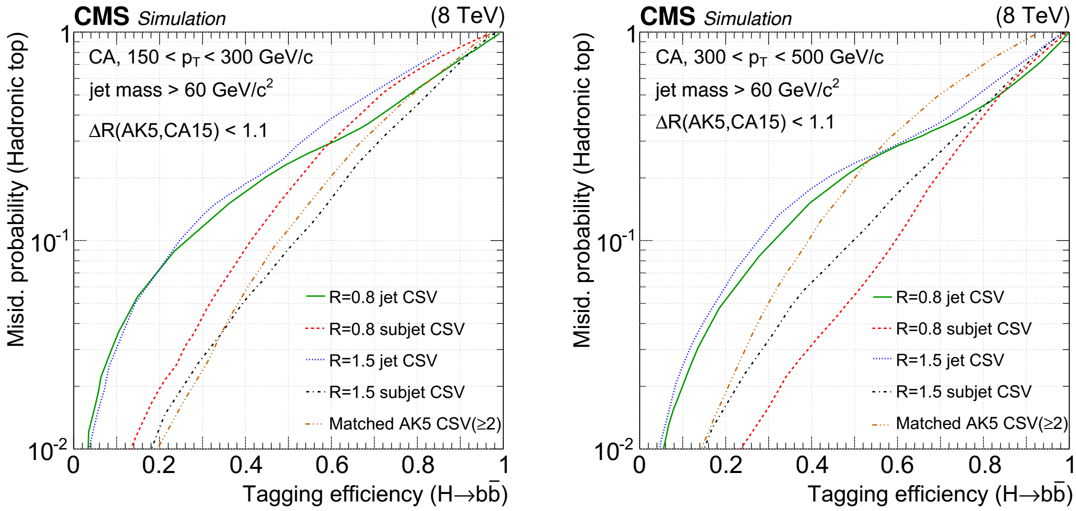

Figure 4. Performance of different H tagging algorithms in simulated signal events, with a signal mass hypothesis of $1000\,\mathrm{GeV}/c^2$. The misidentification probability for the $\mathrm{t\bar{t}}$ background is shown versus the tagging efficiency for boosted Higgs boson decays, for jet transverse momentum ranges of (left) $150 < p_\mathrm{T} < 300\,\mathrm{GeV}/c$ and (right) $300 < p_\mathrm{T} < 500\,\mathrm{GeV}/c$. Different b tagging options are compared: standard b tagging of AK5 jets, subjet b tagging of CA15 and CA8 jets, and b tagging of CA15 jets and CA8 jets. For the case of subjet b tagging, two subjets are required to pass the b tagging criteria. Similarly, two AK5 jets are required to pass the b tagging criteria for standard b tagging.

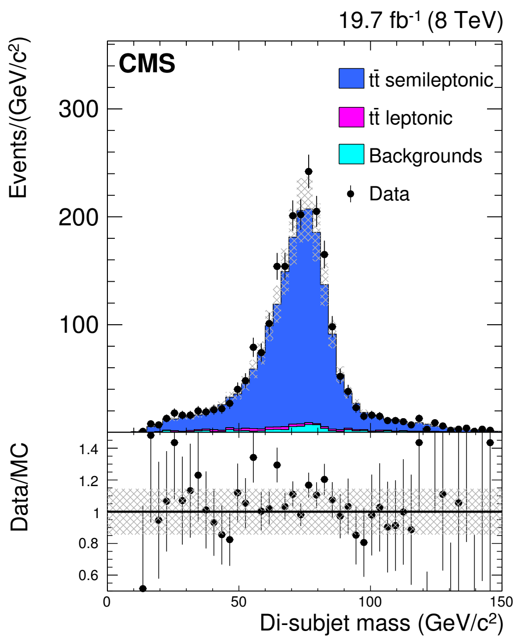

Figure 5. Distribution of the invariant id-subjet mass of a hadronically decaying W boson obtained from a semi-leptonic $\mathrm{t\bar{t}}$ sample. The lower panel shows the ratio of data and simulation. The hatched area indicates the uncertainty in the signal and background cross sections.

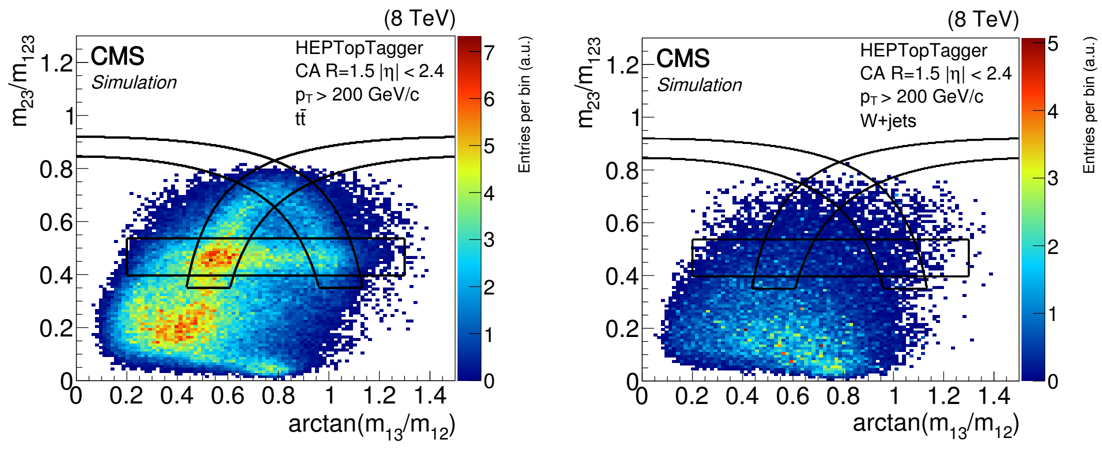

Figure 6. Two-dimensional distributions of m_{23}/m_{123} versus $\arctan(m_{13}/m_{12})$ for HEPTopTagger jets in simulated $t\bar{t}$ events (left) and in simulated background events (right). The simulated background consists of boson+jets, di-boson, single top quark, $t\bar{t}$ all-hadronic, and $t\bar{t}$ leptonic. The area enclosed by the thick solid lines denotes the region selected by the HEPTopTagger.

rithm is applied to each combination of three subjets that are found. The filtering algorithm reclusters the constituents with a variable distance parameter $R_{\text{filt}} = \min(0.3, \Delta R_{ij}/2)$, where i and j are the closest subjets in ΔR in the subjet triplet. The five reclustered subjets with the largest p_{T} are retained and the sum yields the invariant mass of the top quark candidate. The configuration that has an invariant mass closest to the top quark mass is chosen. The constituents of the five leading reclustered subjets are further reclustered using the exclusive CA algorithm, which forces the jet to have exactly three final subjets. The HEPTopTagger uses these three final subjets and selects top quark jets based on the pairwise and three-way subjet masses. Selections are applied in the two-dimensional plane defined by the ratio m_{23}/m_{123} and the arctangent of m_{13}/m_{12}. Here m_{23} is the pairwise mass of the second and third leading subjets. The variables m_{12}, m_{13}, and m_{123} are defined in a similar fashion. The distribution of events in this plane is shown for simulated $t\bar{t}$ events in figure 6 (left) and for a mixture of background (boson+jets, di-boson, single top quark, $t\bar{t}$ all-hadronic, and $t\bar{t}$ leptonic) events in figure 6 (right). A region with a well enhanced structure is only present for $t\bar{t}$ events. The region is highlighted by the thick black lines in figure 6. This structure can be used to suppress backgrounds that do not contain boosted top quarks by rejecting events that lie outside of this region. Additionally, a selection on the top candidate mass, $140 < m_{123} < 250\,\text{GeV}/c^2$, is applied. Another populated region shows up below and to the left of the selected region because of unmerged top decays. This contribution disappears for boosted top quarks above $p_{\mathrm{T}} > 300\,\text{GeV}/c$.

6.2.1 Algorithm performance

The selection criteria used in the algorithm are varied iteratively and the efficiency and mistag rate are calculated for each iteration. The minimum mistag rate for a given signal efficiency is shown in figure 7. The HEPTopTagger curve is determined by fixing the m_{123} selection ($140 < m_{123} < 250\,\text{GeV}/c^2$) and varying the width of the region selected

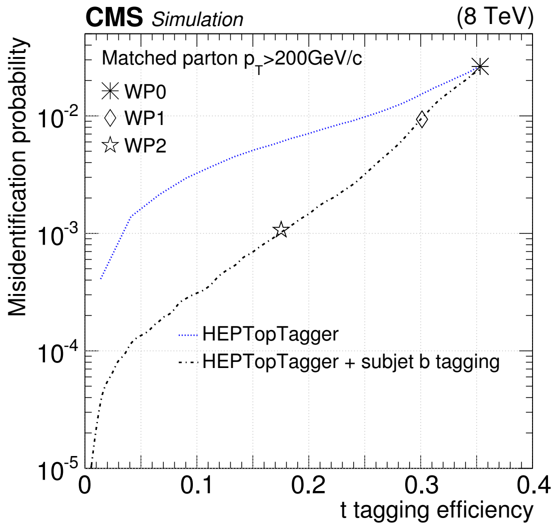

Figure 7. Mistag rate versus t tagging efficiency for the HEPTopTagger and the combination of the HEPTopTagger with subjet b tagging, for CA15 jets matched to generated partons with $p_{\mathrm{T}} > 200\,\mathrm{GeV}/c$. The mistag rate is obtained from simulated QCD multijet events, while the efficiency is determined using simulated $\mathrm{t\bar{t}}$ events.

by the algorithm. The other curve is obtained by applying simultaneously the HEPTopTagger and the subjet b tagging criteria and varying their requirements. Details of these selection criteria are given in ref. [48]. Three working points are defined as indicated by markers in the figure. The working point used in this analysis is WP2, which is defined by the standard HEPTopTagger criteria in addition to a b-tagged subjet identified with the CSVM b tagging algorithm. The other working points (WP1 and WP0) use relaxed HEPTopTagger criteria and relaxed b tagging, and are used to validate the scale factor measurements which are described in the following section.

6.2.2 Scale factors

A semileptonic $\mathrm{t\bar{t}}$ sample is used to study boosted hadronic top quark decays in data. This sample is then used to measure data to simulation scale factors for the t tagging efficiency using WP2. This procedure was introduced in ref. [20]. The $\mathrm{t\bar{t}}$ sample is defined by requiring one muon and at least one b-tagged AK5 jet. Additionally, a top quark candidate CA15 jet is required, with high transverse momentum $p_{\mathrm{T}} > 200\,\mathrm{GeV}/c$ and with at least one b-tagged subjet. This semileptonic selection is very pure and background contributions are negligible. The efficiency of the HEPTopTagger is determined as the fraction of top quark candidate CA15 jets that pass all of the tagging requirements. These measurements yield scale factors ranging from 0.85 to 1.15 depending on the p_{T} and the η of the jet.

7 Event selection

The H_{T} variable used in the analysis is calculated from the transverse momenta of all subjets within the reconstructed CA15 jets with $p_{\mathrm{T}} > 150\,\mathrm{GeV}/c$. This definition is more

T quark mass (GeV/c^2)	production cross section (pb)	expected events	selection efficiency
500	0.59	283.0	2.5%
600	0.174	152.0	4.4%
700	0.059	69.3	6.0%
800	0.021	30.3	7.2%
900	0.0083	12.1	7.3%
1000	0.0034	4.9	7.2%

Table 1. Cross section, expected numbers of selected events, and the selection efficiencies for several signal samples with different values of the T quark mass for an integrated luminosity of $19.7\,\mathrm{fb}^{-1}$. The signal samples assume $\mathcal{B}(\mathrm{T} \to \mathrm{tH}) = 100\%$. The efficiencies are calculated relative to an inclusive sample with no requirements on top quark or Higgs boson decay modes, and without any selection criteria applied.

accurate than that used in the trigger because particle-flow reconstruction is exploited. A threshold of $H_\mathrm{T} > 720\,\mathrm{GeV}/c$ is applied in the offline analysis as the trigger is almost fully efficient above this value. The simulation is corrected to match the data by weighting events based on the ratio between the trigger efficiency calculated in data and in simulation. The systematic uncertainty introduced by this procedure is discussed in section 9.

The full event selection requires the following criteria to be fulfilled:

- At least one CA15 jet must be t-tagged by the HEPTopTagger algorithm and must contain at least one b-tagged subjet (identified by the CSV b tagging algorithm at the medium operating point). The t-tagged jets must have $p_\mathrm{T} > 200\,\mathrm{GeV}/c$.
- At least one CA15 jet must have $p_\mathrm{T} > 150\,\mathrm{GeV}/c$ and must be H-tagged (at least two subjets identified by the CSVM b tagging algorithm). The invariant mass of the two b-tagged subjets has to be larger than $60\,\mathrm{GeV}/c^2$. This jet must not be identical to the top-quark candidate jet.

As mentioned in section 5, the event selection is split further into two categories: single and multiple H tags.

The number of reconstructed CA15 jets predicted by simulation with $p_\mathrm{T} > 150\,\mathrm{GeV}/c$ is shown in the left plot of figure 8, while the right plot shows the number of jets passing the t tagging criteria. In the following figures the hatched regions indicate the statistical uncertainty in the simulated background. The signal hypotheses are represented by the solid and dashed lines.

The impact of subjet b tagging is visible in figure 9. The left plot shows the number of t-tagged CA15 jets with a subjet b tag, while the right plot shows the number of H-tagged jets for events that have at least one t-tagged CA15 jet with a subjet b tag. These figures demonstrate the strong reduction of QCD multijet background by the jet substructure criteria.

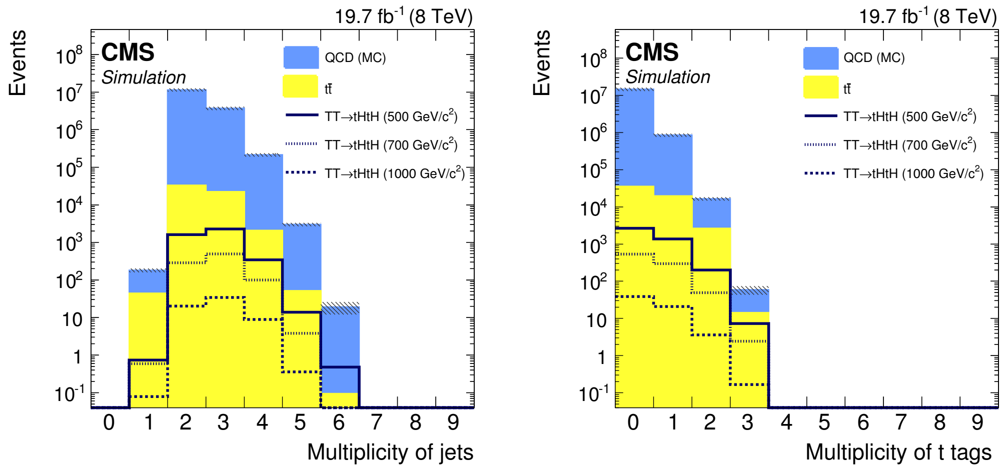

Figure 8. Left: multiplicity of CA15 jets with $p_{\mathrm{T}} > 150\,\mathrm{GeV}/c$. Events with at least two of these jets are selected. Right: multiplicity of CA15 jets with $p_{\mathrm{T}} > 200\,\mathrm{GeV}/c$, that are selected by the HEPTopTagger algorithm. The solid histograms represent the simulated background processes ($\mathrm{t\bar{t}}$ and QCD multijet). The hatched error bands show the statistical uncertainty of the simulated events.

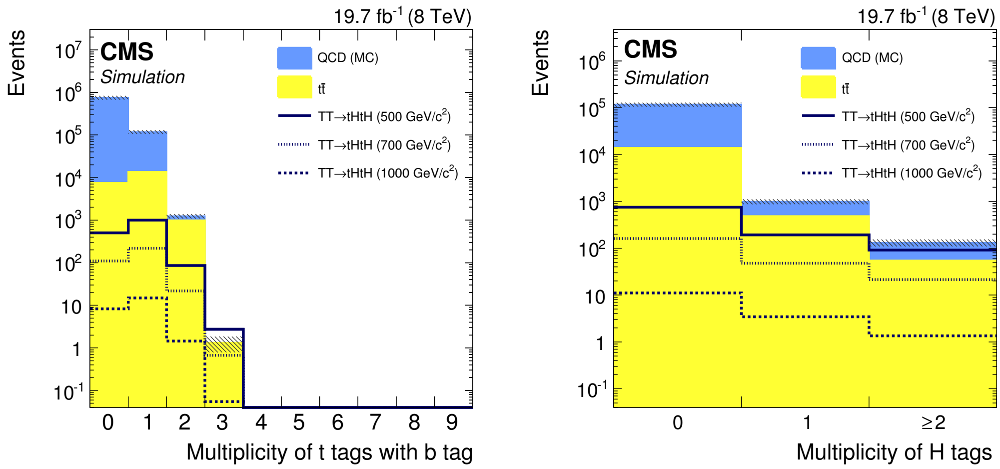

Figure 9. Left: multiplicity of CA15 jets with $p_{\mathrm{T}} > 200\,\mathrm{GeV}/c$ that are tagged by the HEPTopTagger and contain a b-tagged subjet, after requiring at least one jet per event to be selected by the HEPTopTagger algorithm. Right: multiplicity of CA15 jets with $p_{\mathrm{T}} > 150\,\mathrm{GeV}/c$ satisfying the H tagging criteria. Events with three or more H tags are included in the bin with two H tags. The solid histograms represent the simulated background processes ($\mathrm{t\bar{t}}$ and QCD multijet). The hatched error bands show the statistical uncertainty of the simulated events.

The number of selected events for each signal sample of the benchmark model and the selection efficiencies, derived from simulated events, are given in table 1.

8 Background estimation

The $\mathrm{t\bar{t}}$ background is evaluated from simulated events, corrected for differences between data and simulation in b tagging and trigger efficiencies described above. The uncertainties in the normalization and shape of $t\bar{t}$ events are discussed in section 9. Background contributions from ttH and hadronically decaying W/Z plus heavy flavour processes are found to be below 1% and are neglected.

The QCD multijet background is estimated in data using a two-dimensional sideband extrapolation. In this method, two uncorrelated criteria in the event selection are inverted to obtain sideband regions that are enriched in QCD multijet events and depleted in signal events. Inverting each criterion individually, as well as both at the same time, results in three exclusive sideband regions, denoted A, B and C:

- Sideband region B is obtained by inverting the selection criteria of the HEPTopTagger algorithm. The top quark mass window as well as all requirements on the pairwise subjet mass in the HEPTopTagger are inverted. Events outside of the selected region shown in figure 6 (section 6) are used to define the inverted HEPTopTagger control region, while the events that are inside define the signal region. Details of these selection criteria of the HEPTopTagger are given in section 6 and [48].

- Sideband region C is obtained by inverting the H tagging algorithm. Only events with zero H tags are selected and the requirement on the pairwise subjet mass is removed.

- Sideband region A is obtained by inverting both the H tagging and the t tagging algorithms as described above.

- Events in the signal region D have all tagging requirements applied.

The $t\bar{t}$ contamination in the sideband regions amounts to a maximum of 8% in region C. This is accounted for by subtracting the $t\bar{t}$ contribution predicted by the simulation in each of the sideband regions. Backgrounds due to ttH and hadronically decaying W/Z plus heavy flavour processes are found to have a negligible contribution in the sideband regions. A signal injection test has been performed to evaluate the impact of a hypothetical signal on the background model. It has been found that the signal contamination in the sideband regions leads to a small effect of less than 1.4% for $m_{\mathrm{T}} = 700\ \mathrm{GeV}/c^2$ on the measured QCD multijet event rate, and therefore the possible signal contamination in the sideband regions is neglected in the analysis.

The QCD multijet yield in the signal region is calculated as

$$R_D = R_B \frac{R_C}{R_A}, \tag{8.1}$$

where R_A denotes the rate of events in sideband A. The $t\bar{t}$ contamination in the sideband regions is subtracted. The event rates in the three sideband regions and the signal region are provided in table 2. The resulting predictions of the QCD multijet backgrounds are given in table 3 for the two event categories.

The closure of this method is verified with simulated QCD multijet events. As the method assumes the selection criteria defining the sideband regions to be uncorrelated, the

		single H tag category		multi H tag category	
region A		region B		region B	
data	1152640	data	8384	data	1157
data $-$ $\mathrm{t\bar{t}}$	1146464	data $-$ $\mathrm{t\bar{t}}$	8089	data $-$ $\mathrm{t\bar{t}}$	1123
region C		region D		region D	
data	140911				
data $-$ $\mathrm{t\bar{t}}$	129972	prediction	917 ± 11	prediction	127 ± 4

Table 2. Event rates in the signal and sideband regions obtained from the two-dimensional sideband extrapolation in data for the two H tag categories. The $\mathrm{t\bar{t}}$ contamination is subtracted from the nominal yield in the sideband regions. The prediction of the QCD multijet event rate in the signal region D is given along with statistical uncertainties that arise from the limited size of event samples in the sideband regions. The sideband regions A and C are common to both H tag multiplicity categories.

	single H tag category	multi H tag category
QCD (predicted from data)	917 ± 11	127 ± 4
$\mathrm{t\bar{t}}$ (from simulation)	486 ± 8	55 ± 3
total background	1403 ± 14	182 ± 5
data	1355	205

Table 3. Predicted background contributions in the signal region for the two event categories with one and with multiple H tags. Statistical uncertainties in the background estimates are also shown.

following condition must be fulfilled:

$$\frac{R_A}{R_B} = \frac{R_C}{R_D}. \tag{8.2}$$

According to simulation, the ratios are $R_A/R_B = 185{\pm}5$ ($1417{\pm}97$) and $R_C/R_D = 185{\pm}17$ (1203 ± 250) for the single (multi) H tag event category. The quoted uncertainties are statistical. It can be seen that the ratios agree within the statistical uncertainties. The largest uncertainties occur in the R_C/R_D ratio and are about 10 (20)% for the single (multi) H tag category.

In addition to the event yields, the shapes of the H_T and $m_{\mathrm{b\bar{b}}}$ distributions for the QCD multijet processes are also derived from the sideband regions. For both the H_T and $m_{\mathrm{b\bar{b}}}$ variables the sideband region B (inverted t tagger) is used. The expected contribution from $\mathrm{t\bar{t}}$ events is subtracted from the sideband.

Closure is also verified for the shape of H_T and $m_{\mathrm{b\bar{b}}}$ distributions in the signal and sideband regions. Figure 10 shows a comparison of the H_T and $m_{\mathrm{b\bar{b}}}$ shapes in the sideband and signal regions for the single and the multiple H tag event categories. The distributions agree within statistical uncertainties.

The method has also been validated in data. The shapes of the simulated H_T and $m_{\mathrm{b\bar{b}}}$ distributions in the signal region agree well with the predicted distributions in data.

JHEP06(2015)080

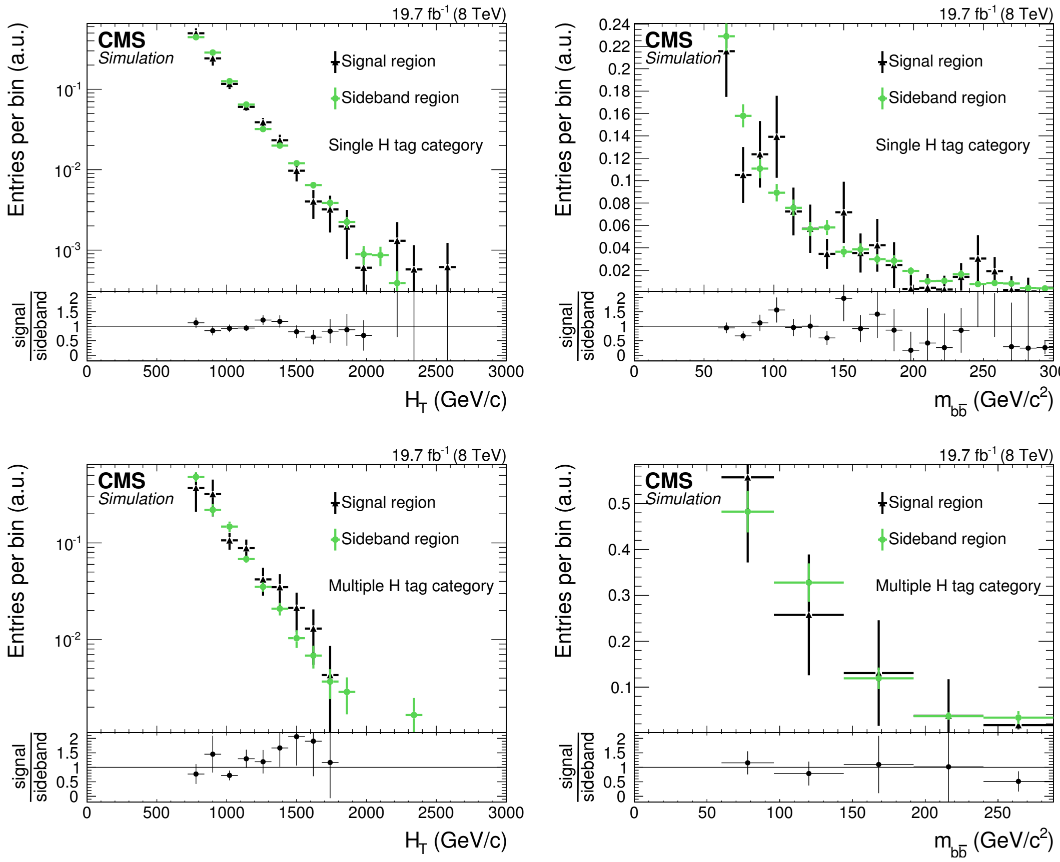

Figure 10. Comparison of the H_T (left) and $m_{\mathrm{b}\bar{\mathrm{b}}}$ (right) distributions in the sideband region B and signal region for the single (top) and multiple (bottom) H tag event categories for simulated QCD multijet events. All distributions are normalized to unity for shape comparison. The lower panels in the figures show the ratio of the signal and sideband regions.

The absolute rate of events shows a disagreement between simulation and the data-derived rate of a factor of two. This disagreement is taken into account when assigning systematic uncertainties in the background, as explained in section 9.

9 Systematic uncertainties

As the analysis relies on simulation for the $\mathrm{t}\bar{\mathrm{t}}$ background prediction, a careful evaluation of uncertainties affecting both the normalization and shape of the $\mathrm{t}\bar{\mathrm{t}}$ background events is needed. This is also required for the simulated signal events.

The QCD multijet background is obtained from data. The rate and shape of the $\mathrm{t}\bar{\mathrm{t}}$ background have an effect on the measurement of the QCD multijet background because the $\mathrm{t}\bar{\mathrm{t}}$ contamination in the sideband region is subtracted from data.

The detailed list of systematic uncertainties is given below. Most of these uncertainties have an impact on both the shapes and normalization of the sensitive variables H_T and $m_{\mathrm{b}\bar{\mathrm{b}}}$, while the uncertainty in the integrated luminosity only affects the normalization. The uncertainties are summarized in table 4.

JHEP06(2015)080

- b tagging scale factor uncertainties: based on the measurements described in section 6.1 and ref. [49], scale factors with their corresponding uncertainties are applied to simulated samples. The scale factor uncertainties for the b tagging efficiency depend on p_{T} and η. The typical size of these uncertainties is between 1 and 2% while the mistag rate uncertainty is around 15%. The b tagging scale factor uncertainties affect both the normalization and shape of the $\mathrm{t\bar{t}}$ background and signal events. Depending on the sample and signal mass point, the impact of the b tagging scale factor uncertainty on the expected number of selected signal and $\mathrm{t\bar{t}}$ events is 5 to 8% while the impact of the mistag scale factor uncertainty is 0.3 to 4%.

- HEPTopTagger scale factor uncertainty: the efficiency of the HEPTopTagger has been measured and compared to simulation to derive scale factors as described in section 6.2. The uncertainties in these scale factor measurements are between 3 and 6%, and are parameterized as a function of p_{T}. These uncertainties affect both the normalization and shape of the $\mathrm{t\bar{t}}$ background and signal events. The impact on the expected number of signal and $\mathrm{t\bar{t}}$ events is 0.4 to 2.3%.

- Jet energy corrections: dedicated energy corrections for CA15 jets are not available. Therefore, the energy corrections for jets reconstructed with the anti-k_{T} algorithm with size parameter $R = 0.7$ (AK7) [26] have been used [43]. It has been verified that these corrections are valid by comparing the reconstructed jets in simulation to the corresponding generator level jets where exactly the same clustering and grooming algorithms have been applied. The ratio between reconstructed and generated momentum for these jets is found to be consistent with unity, with variations that are less than 4%. The impact of the uncertainty on the jet energy scale of filtered CA15 jets is evaluated by varying the jet four-momentum up and down by the jet energy scale uncertainties of AK7 jets, with an additional 4% systematic uncertainty. The uncertainty in the subjet energy scale is assumed to be similar to the energy scale uncertainty of AK5 jets. The impact on the expected number of selected $\mathrm{t\bar{t}}$ and signal events is less than 0.5% for CA15 jets and less than 5% for subjets.

- PDF uncertainties: simulated $\mathrm{t\bar{t}}$ events are weighted according to the uncertainties parameterized by the CTEQ6 eigenvectors [36]. The shifts produced by the individual eigenvectors are added in quadrature in each bin of the H_{T} and $m_{\mathrm{b\bar{b}}}$ distributions. The resulting uncertainty in the number of expected $\mathrm{t\bar{t}}$ events ranges from 2.4 to 8%.

- Scale uncertainties: the impact of the renormalization and factorization scale uncertainties on the $\mathrm{t\bar{t}}$ simulation has been studied using $\mathrm{t\bar{t}}$ event samples generated with two different values of these scales (moving them simultaneously up or down by a factor of two relative to the nominal value). It has been verified that this uncertainty has no impact on the shapes of H_{T} and $m_{\mathrm{b\bar{b}}}$ distributions within the statistical uncertainties of the simulated samples. The resulting impact on the selected number of $\mathrm{t\bar{t}}$ events is 34%.

- QCD multijet background normalization: the normalization and shape of QCD multijet events do not show any discrepancy between the predicted and observed shapes in the signal region based on the closure test with simulated events, as discussed in section 8. The comparison of the simulated sidebands with data shows a very good agreement of the shapes as well, but the normalization is not in agreement. Therefore a systematic uncertainty in the normalization of QCD multijet events is taken into account. This uncertainty is derived from the statistical precision of the closure test, which is limited by the finite size of simulated event samples. The uncertainty in the single H tag category is 10% while the uncertainty is 20% in the multi H tag category. The only systematic uncertainty in the shape of the QCD multijet background arises from the subtraction of $t\bar{t}$ events. The effect of the $t\bar{t}$ scale uncertainty on the estimation of the QCD multijet background is less than 1%. Uncertainties in the $t\bar{t}$ simulation and the corresponding propagated uncertainties in the QCD multijet prediction are treated as correlated, but they have opposite effects.

- Trigger reweighting: a scale factor SF_{trig} is applied to correct for the different behaviour between data and simulation in the region in which the trigger is not fully efficient. A systematic uncertainty in the scale factor is obtained by varying SF_{trig} by $\pm 0.5(1 - SF_{\mathrm{trig}})$. This uncertainty does not affect the plateau region of the trigger, where $SF_{\mathrm{trig}} = 1$. This uncertainty is taken into account both as a shape and as a rate uncertainty. It only affects the low-H_{T} range. The trigger efficiency is measured in a $t\bar{t}$-enriched data sample. For $720 < H_{\mathrm{T}} \leq 780\,\mathrm{GeV}/c$ the efficiency is 75%, with a SF_{trig} of 80%. For $780 < H_{\mathrm{T}} \leq 840\,\mathrm{GeV}/c$ the trigger efficiency is 93%, with a SF_{trig} of 94%. For $H_{\mathrm{T}} > 840\,\mathrm{GeV}/c$ the trigger has an efficiency always greater than 99% and a SF_{trig} consistent with one. The overall impact of this uncertainty on the event yield is 3.5%.

- Luminosity: an uncertainty in the integrated luminosity of 2.6% is taken into account [50].

- Cross section of the $t\bar{t}$ background: an uncertainty of 13% is assigned to the $t\bar{t}$ cross section. This uncertainty is obtained with the technique used in the differential $t\bar{t}$ cross section measurement [51] for large invariant mass values of the $t\bar{t}$ system.

10 Results

Figure 11 shows the comparison between data and the expected background contributions for the single and multiple H tag event categories after all event selection criteria are applied. In the multiple H tag category only the Higgs boson candidate with the highest transverse momentum is used. The QCD multijet background has been derived from data as discussed in section 8. Signal samples at three different mass points are also shown. In these plots only signal samples in which all T quarks decay into a top quark and a Higgs boson are shown.

uncertainty	$t\bar{t}$	QCD multijet	signal 500 GeV/c^2	signal 700 GeV/c^2	signal 1000 GeV/c^2
b tagging:					
heavy flavour	$+9.2/-7.5$	—	$+6.0/-6.8$	$+7.1/-6.5$	$+7.8/-8.0$
light flavour	$+4.2/-3.2$	—	$+1.2/-0.7$	$+0.9/-0.6$	$+0.8/-1.0$
HEPTopTagger	$+0.9/-0.4$	—	$+1.6/-1.7$	$+1.7/-1.8$	$+1.8/-2.3$
jet energy corrections	$+5.0/-4.1$	—	$+3.7/-2.8$	$+0.7/-0.7$	$+0.1/-0.4$
scale uncertainties	± 34	—	—	—	—
PDF	$+8.0/-4.4$	—	—	—	—
trigger scale factors	$+3.6/-4.0$	—	$+2.3/-2.3$	$+0.7/-0.7$	$+0.06/-0.08$
luminosity	± 2.6	—	± 2.6	± 2.6	± 2.6
$t\bar{t}$ cross section	± 13	—	—	—	—
background estimate:					
single H tag	—	± 10	—	—	—
multi H tag	—	± 20	—	—	—

Table 4. Systematic uncertainties and their effect on signal and background processes, expressed in percent. The uncertainties are described in detail in section 9. This table shows uncertainties in the normalization only.

Based on the expected distributions for the background and signal models for H_T and $m_{b\bar{b}}$, a discriminating quantity L is calculated for each event, where

$$L = \ln\left(1 + \frac{P_{\rm sig}(H_T)}{P_{\rm back}(H_T)}\frac{P_{\rm sig}(m_{b\bar{b}})}{P_{\rm back}(m_{b\bar{b}})}\right). \tag{10.1}$$

The P variables represent the probability densities for the signal or background hypotheses. The $P_{\rm back}$ values are obtained from the sum of the simulated $t\bar{t}$ and QCD multijet background distributions because other background contributions are found to be negligible, as discussed in section 8. For the signal hypothesis, the $P_{\rm sig}$ values are obtained from simulated H_T and $m_{b\bar{b}}$ distributions for each signal mass point. A binned likelihood method is used where the values for the P variables are taken from histograms. The distribution of this variable is shown in figure 12 for data compared to the background prediction and signal hypotheses, for both the single and multiple H tag categories. As the signal model is included in the discriminator, each signal mass hypothesis has its own definition of L. The mass points 500, 700, and 1000 GeV/c^2 are shown in these figures. The spikes in these distributions are due to the likelihood definition, that is obtained by taking values from binned distributions.

No signal-like excess is observed in data. Bayesian upper limits [52] on the T quark production cross section are obtained with the Theta framework [53]. The nuisance parameters are assigned to the sources of systematic uncertainties reported in section 9, which are taken into account as global normalization uncertainties and as shape uncertainties where applicable. The shape uncertainties are taken into account by interpolating between

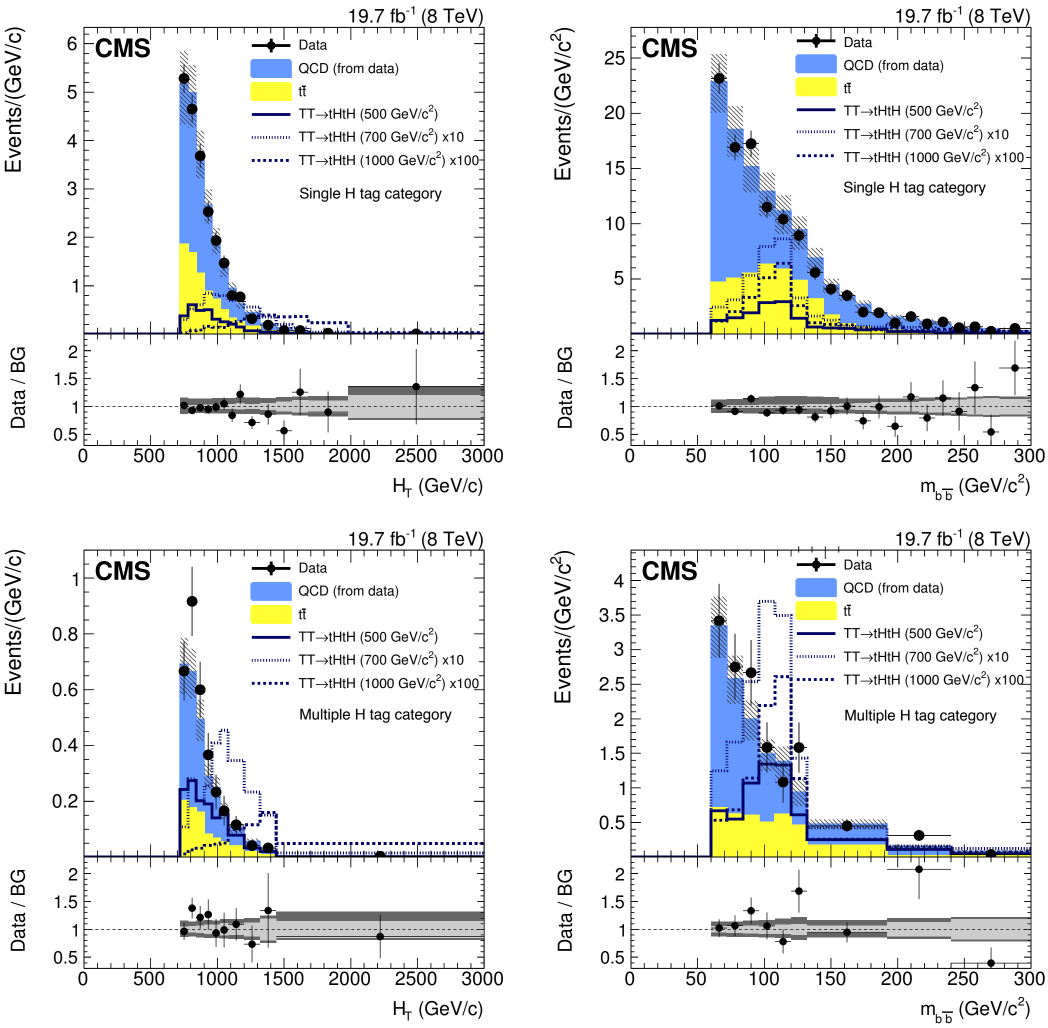

Figure 11. The H_{T} (left) and Higgs boson candidate mass (right) distributions for the single H tag category (top) and the multiple H tag category (bottom). The QCD multijet background is derived from data. The $\mathrm{t\bar{t}}$ background is taken from simulation. The hypothetical signal is shown for three different mass points: 500, 700, and 1000 GeV/c^2. The hatched error bands show the quadratic sum of all systematic and statistical uncertainties in the background. In the ratio plot, the statistical uncertainty in the background is depicted by the inner central band, while the outer band shows the quadratic sum of all systematic and statistical uncertainties.

the nominal and $\pm 1\,\sigma$ templates of the likelihood distributions. Figure 13 shows the observed and expected limits on the T pair production cross section, for the hypothesis of an exclusive branching fraction $\mathcal{B}(\mathrm{T} \to \mathrm{tH}) = 100\%$ using the combination of both the single and multiple H tag event categories. T quarks exclusively decaying into tH and with mass values below 745 GeV/c^2 are excluded at 95% confidence level (CL), with an expected exclusion limit of 773 GeV/c^2. Due to the lower background contamination, the multiple H tag event category provides the largest contribution to the achieved sensitivity.

In evaluating limits, the other decay modes of the T quark must be considered. For mixed branching fractions there are six distinct final states: tHtH, tHtZ, tHbW, bWbW,

JHEP06(2015)080

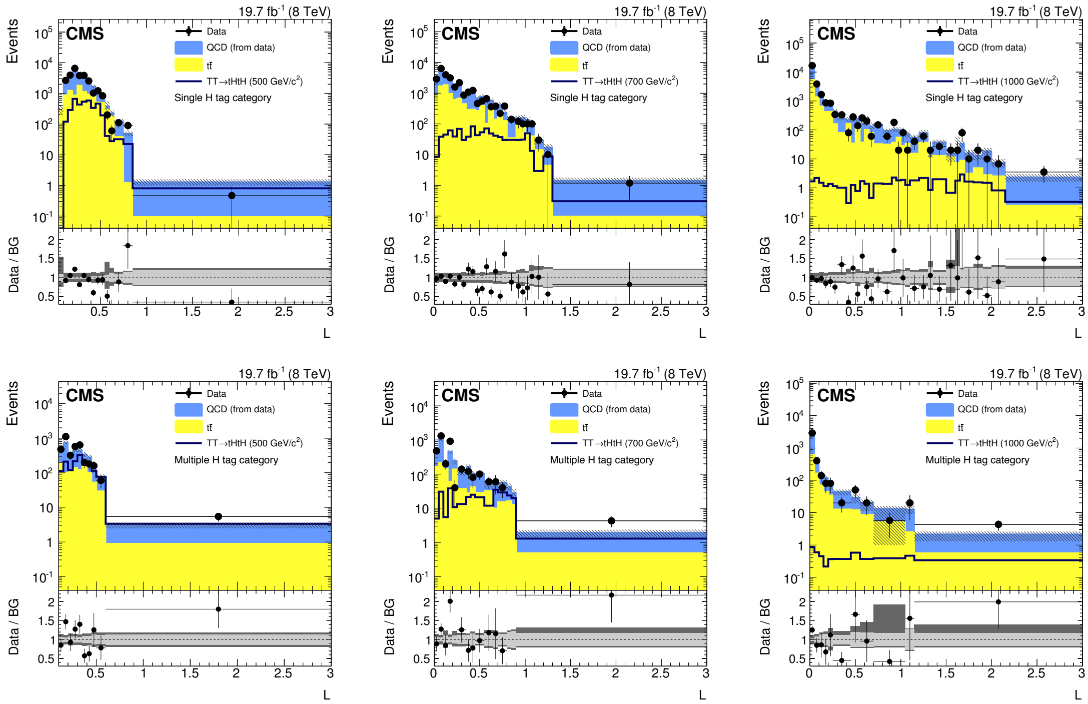

Figure 12. Discriminating variable L constructed from both H_{T} and $m_{\mathrm{b\bar{b}}}$ for the single (top) and the multiple (bottom) H tag categories. The three signal hypotheses with 500, 700, and 1000 GeV/c^2 are shown on the left, middle, and right, respectively. The QCD multijet background is derived from data. The $\mathrm{t\bar{t}}$ background is derived from simulation. The hatched error bands show the quadratic sum of all systematic and statistical uncertainties in the background. In the ratio plot, the statistical uncertainty in the background is depicted by the inner central band, while the outer band shows the quadratic sum of all systematic and statistical uncertainties.

bWtZ, tZtZ. Three of these final states contain at least one tH decay. This means that the single H tag category of this analysis is sensitive also to non-exclusive branching fractions. Furthermore, we also expect some sensitivity to tZ decays because the mass of the Z boson differs from the mass of the Higgs boson by only 35 GeV/c^2 and because it decays into b quark pairs with a branching fraction of 15.6%. A selection efficiency of 4.5% is found for the tHtZ final state, 3% for tHbW, and 2% for tZtZ for a T quark mass of 800 GeV/c^2. These efficiencies are calculated in the same way as those for tHtH in table 1.

A dedicated optimization is not performed for the non-exclusive decay modes. Nevertheless, exclusion limits are calculated for all branching fractions from a scan of all allowed values. Simulated signal samples have been produced for each set of branching fractions used in the scan.

Observed and expected lower limits on the mass of the T quark for different branching fractions are listed in table 5 and shown in figure 14. Table 5 shows only those branching fractions for which actual mass limits exist (where the theory curve crosses the limit curve). A good sensitivity is achieved for T → tH branching fractions down to 80%. The observed and expected limits on the production cross section for different branching fractions are given in table 6 and shown in figure 15.

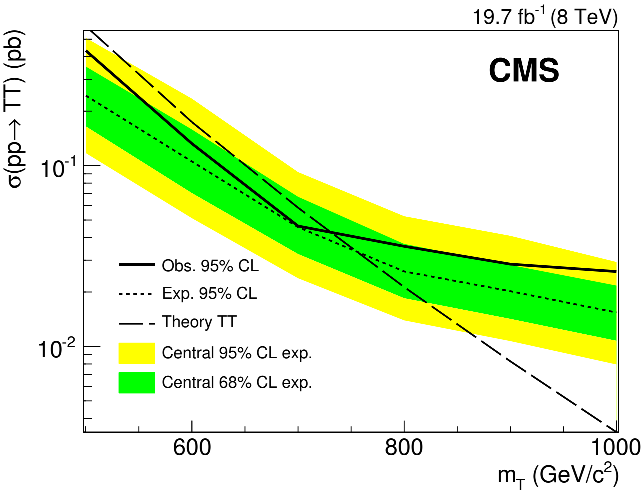

Figure 13. Observed (solid line) and expected (dotted line) Bayesian upper limits on the T quark production cross section determined from the variable L for the combination of the single and multiple H tag categories, for the hypothesis of an exclusive branching fraction $\mathcal{B}(\mathrm{T} \to \mathrm{tH}) = 100\%$. The green (inner) and yellow (outer) bands show the $1\,\sigma$ $(2\,\sigma)$ uncertainty ranges, respectively. The dashed line shows the prediction of the theory as discussed in section 3.

bW	tZ	tH	observed limit	expected limit	expected$\pm 1\sigma$	expected$\pm 2\sigma$
0.0	0.2	0.8	698	732	[596,795]	[<500,851]
0.0	0.15	0.85	715	734	[633,798]	[<500,857]
0.0	0.1	0.9	725	751	[639,806]	[<500,862]
0.0	0.05	0.95	739	763	[655,827]	[538,873]
0.0	0.0	1.0	745	773	[664,832]	[557,875]
0.05	0.1	0.85	716	732	[619,798]	[<500,856]
0.05	0.05	0.9	724	749	[633,812]	[503,858]
0.05	0.0	0.95	731	757	[650,817]	[534,865]
0.1	0.05	0.85	708	730	[595,795]	[<500,849]
0.1	0.0	0.9	720	737	[599,799]	[<500,859]

Table 5. Observed and expected lower limits on the mass of the T quark (in GeV/c^2) for a range of T quark branching fraction hypotheses listed in the first three columns. Only combinations for which an observed limit is found are reported. When the limit lies below the scanned mass region between 500 and 1000 GeV/c^2 a value of < 500 is indicated.

11 Summary

A search for heavy resonances decaying to top quarks and Higgs bosons has been performed using proton-proton collisions recorded with the CMS detector at $\sqrt{s} = 8$ TeV, corresponding to an integrated luminosity of 19.7 fb^{-1}. The benchmark model considered is a heavy vector-like T quark that decays into bW, tZ, and tH in all-hadronic final states. The anal-

JHEP06(2015)080

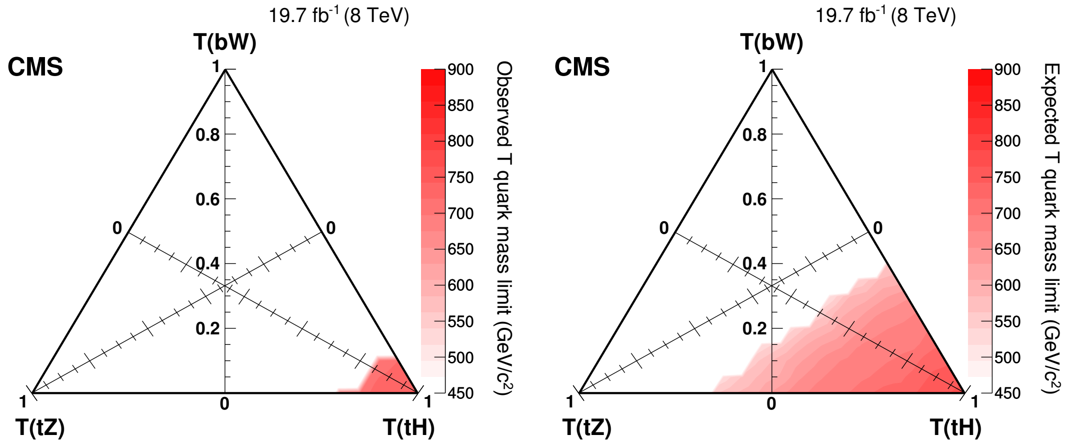

Figure 14. Branching fraction triangle with observed upper limits (left) and expected limits (right) for the T quark mass. Every point in the triangle corresponds to a particular set of branching fraction values subject to the constraint that all three add up to one. The branching fraction for each mode decreases from one at the corner labelled with the specific decay mode to zero at the opposite side of the triangle.

bW	tZ	tH	500	600	700	800	900	1000
			0.432	0.132	0.046	0.036	0.029	0.026
0	0	1	$0.244^{+0.109}_{-0.079}$	$0.105^{+0.053}_{-0.035}$	$0.046^{+0.021}_{-0.014}$	$0.026^{+0.011}_{-0.008}$	$0.020^{+0.008}_{-0.006}$	$0.015^{+0.007}_{-0.004}$
			0.576	0.157	0.059	0.046	0.036	0.029
0	0.2	0.8	$0.299^{+0.124}_{-0.100}$	$0.118^{+0.063}_{-0.036}$	$0.054^{+0.025}_{-0.014}$	$0.032^{+0.014}_{-0.010}$	$0.023^{+0.011}_{-0.006}$	$0.018^{+0.008}_{-0.005}$
			0.866	0.191	0.076	0.057	0.043	0.036
0	0.4	0.6	$0.389^{+0.210}_{-0.122}$	$0.143^{+0.074}_{-0.043}$	$0.067^{+0.027}_{-0.019}$	$0.041^{+0.019}_{-0.012}$	$0.030^{+0.014}_{-0.009}$	$0.023^{+0.010}_{-0.007}$
			0.656	0.155	0.061	0.049	0.038	0.033
0.2	0	0.8	$0.340^{+0.174}_{-0.110}$	$0.137^{+0.062}_{-0.043}$	$0.061^{+0.027}_{-0.018}$	$0.035^{+0.015}_{-0.010}$	$0.026^{+0.011}_{-0.008}$	$0.020^{+0.009}_{-0.006}$
			0.934	0.206	0.081	0.060	0.049	0.039
0.2	0.2	0.6	$0.459^{+0.241}_{-0.150}$	$0.165^{+0.080}_{-0.052}$	$0.076^{+0.033}_{-0.022}$	$0.045^{+0.019}_{-0.014}$	$0.033^{+0.014}_{-0.010}$	$0.025^{+0.011}_{-0.007}$

Table 6. Branching fractions (first three columns) and the observed and expected upper limits on the cross section for different mass values of the T quark. The expected limits are quoted with their corresponding uncertainties while the observed limits are quoted without uncertainties. The cross section limits are given in units of pb, while the T quark mass values are given in units of GeV/c^2.

ysis makes use of jet substructure techniques including algorithms for the identification of boosted top quarks, boosted Higgs bosons, and subjet b tagging. Results are presented for exclusive T quark decay modes as well as for non-exclusive branching fractions. If the heavy T quark has a branching fraction of 100% for T $\rightarrow$ tH, the observed (expected) exclusion limit on the mass of the T quark is 745 (773) GeV/c^2 at 95% confidence level. This limit is similar to that obtained from leptonic final states [14]. These results are the first to exploit the all-hadronic final state in the search for vector-like quarks and they facilitate the combination with other analyses to improve the mass reach.

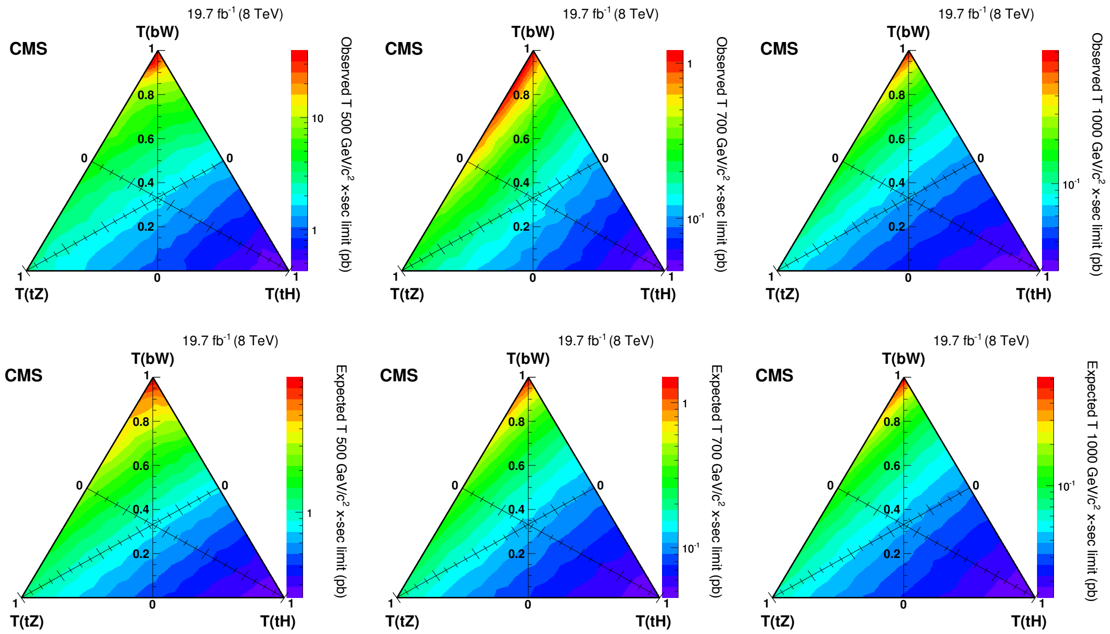

Figure 15. Branching fraction triangle with observed (top) and expected (bottom) limits on the T quark pair production cross section for three different T quark mass hypotheses: 500 (left), 700 (middle), and 1000 GeV/c^2 (right). Every point in the triangle corresponds to a particular set of branching fraction values subject to the constraint that all three add up to one. The branching fraction for each mode decreases from one at the corner labelled with the specific decay mode to zero at the opposite side of the triangle.

Acknowledgments

We congratulate our colleagues in the CERN accelerator departments for the excellent performance of the LHC and thank the technical and administrative staffs at CERN and at other CMS institutes for their contributions to the success of the CMS effort. In addition, we gratefully acknowledge the computing centres and personnel of the Worldwide LHC Computing Grid for delivering so effectively the computing infrastructure essential to our analyses. Finally, we acknowledge the enduring support for the construction and operation of the LHC and the CMS detector provided by the following funding agencies: BMWFW and FWF (Austria); FNRS and FWO (Belgium); CNPq, CAPES, FAPERJ, and FAPESP (Brazil); MES (Bulgaria); CERN; CAS, MoST, and NSFC (China); COLCIENCIAS (Colombia); MSES and CSF (Croatia); RPF (Cyprus); MoER, ERC IUT and ERDF (Estonia); Academy of Finland, MEC, and HIP (Finland); CEA and CNRS/IN2P3 (France); BMBF, DFG, and HGF (Germany); GSRT (Greece); OTKA and NIH (Hungary); DAE and DST (India); IPM (Iran); SFI (Ireland); INFN (Italy); MSIP and NRF (Republic of Korea); LAS (Lithuania); MOE and UM (Malaysia); CINVESTAV, CONACYT, SEP, and UASLP-FAI (Mexico); MBIE (New Zealand); PAEC (Pakistan); MSHE and NSC (Poland); FCT (Portugal); JINR (Dubna); MON, RosAtom, RAS and RFBR (Russia); MESTD (Serbia); SEIDI and CPAN (Spain); Swiss Funding Agencies (Switzerland); MST (Taipei); ThEPCenter, IPST, STAR and NSTDA (Thailand); TUBITAK and TAEK (Turkey); NASU and SFFR (Ukraine); STFC (United Kingdom); DOE and NSF (U.S.A.).

JHEP06(2015)080

Individuals have received support from the Marie-Curie programme and the European Research Council and EPLANET (European Union); the Leventis Foundation; the A. P. Sloan Foundation; the Alexander von Humboldt Foundation; the Belgian Federal Science Policy Office; the Fonds pour la Formation à la Recherche dans l'Industrie et dans l'Agriculture (FRIA-Belgium); the Agentschap voor Innovatie door Wetenschap en Technologie (IWT-Belgium); the Ministry of Education, Youth and Sports (MEYS) of the Czech Republic; the Council of Science and Industrial Research, India; the HOMING PLUS programme of the Foundation for Polish Science, cofinanced from European Union, Regional Development Fund; the Compagnia di San Paolo (Torino); the Consorzio per la Fisica (Trieste); MIUR project 20108T4XTM (Italy); the Thalis and Aristeia programmes cofinanced by EU-ESF and the Greek NSRF; and the National Priorities Research Program by Qatar National Research Fund.

References

[1] CMS collaboration, *Observation of a new boson at a mass of* 125 *GeV with the CMS experiment at the LHC*, *Phys. Lett.* **B 716** (2012) 30 [arXiv:1207.7235] [INSPIRE].

[2] ATLAS collaboration, *Observation of a new particle in the search for the standard model Higgs boson with the ATLAS detector at the LHC*, *Phys. Lett.* **B 716** (2012) 1 [arXiv:1207.7214] [INSPIRE].

[3] N. Arkani-Hamed, A.G. Cohen and H. Georgi, *Electroweak symmetry breaking from dimensional deconstruction*, *Phys. Lett.* **B 513** (2001) 232 [hep-ph/0105239] [INSPIRE].

[4] M. Schmaltz and D. Tucker-Smith, *Little Higgs review*, *Ann. Rev. Nucl. Part. Sci.* **55** (2005) 229 [hep-ph/0502182] [INSPIRE].

[5] I. Antoniadis, K. Benakli and M. Quirós, *Finite Higgs mass without supersymmetry*, *New J. Phys.* **3** (2001) 20 [hep-th/0108005] [INSPIRE].

[6] Y. Hosotani, S. Noda and K. Takenaga, *Dynamical gauge-Higgs unification in the electroweak theory*, *Phys. Lett.* **B 607** (2005) 276 [hep-ph/0410193] [INSPIRE].

[7] K. Agashe, R. Contino and A. Pomarol, *The minimal composite Higgs model*, *Nucl. Phys.* **B 719** (2005) 165 [hep-ph/0412089] [INSPIRE].

[8] O. Eberhardt et al., *Joint analysis of Higgs decays and electroweak precision observables in the standard model with a sequential fourth generation*, *Phys. Rev.* **D 86** (2012) 013011 [arXiv:1204.3872] [INSPIRE].

[9] J.A. Aguilar-Saavedra, R. Benbrik, S. Heinemeyer and M. Pérez-Victoria, *Handbook of vectorlike quarks: mixing and single production*, *Phys. Rev.* **D 88** (2013) 094010 [arXiv:1306.0572] [INSPIRE].

[10] CMS collaboration, *Search for pair produced fourth-generation up-type quarks in pp collisions at* $\sqrt{s} = 7$ *TeV with a lepton in the final state*, *Phys. Lett.* **B 718** (2012) 307 [arXiv:1209.0471] [INSPIRE].

JHEP06(2015)080

[11] CMS collaboration, *Search for heavy, top-like quark pair production in the dilepton final state in pp collisions at $\sqrt{s} = 7$ TeV*, Phys. Lett. **B 716** (2012) 103 [arXiv:1203.5410] [INSPIRE].

[12] ATLAS collaboration, *Search for pair production of heavy top-like quarks decaying to a high-p_T W boson and a b quark in the lepton plus jets final state at $\sqrt{s} = 7$ TeV with the ATLAS detector*, Phys. Lett. **B 718** (2013) 1284 [arXiv:1210.5468] [INSPIRE].

[13] CMS collaboration, *Search for a vector-like quark with charge 2/3 in $t + Z$ events from pp collisions at $\sqrt{s} = 7$ TeV*, Phys. Rev. Lett. **107** (2011) 271802 [arXiv:1109.4985] [INSPIRE].

[14] CMS collaboration, *Inclusive search for a vector-like T quark with charge $\frac{2}{3}$ in pp collisions at $\sqrt{s} = 8$ TeV*, Phys. Lett. **B 729** (2014) 149 [arXiv:1311.7667] [INSPIRE].

[15] G.D. Kribs, A. Martin and T.S. Roy, *Higgs boson discovery through top-partners decays using jet substructure*, Phys. Rev. **D 84** (2011) 095024 [arXiv:1012.2866] [INSPIRE].

[16] J.M. Butterworth, A.R. Davison, M. Rubin and G.P. Salam, *Jet substructure as a new Higgs search channel at the LHC*, Phys. Rev. Lett. **100** (2008) 242001 [arXiv:0802.2470] [INSPIRE].

[17] D.E. Kaplan, K. Rehermann, M.D. Schwartz and B. Tweedie, *Top tagging: a method for identifying boosted hadronically decaying top quarks*, Phys. Rev. Lett. **101** (2008) 142001 [arXiv:0806.0848] [INSPIRE].

[18] CMS collaboration, *A Cambridge-Aachen (C-A) based jet algorithm for boosted top-jet tagging*, CMS-PAS-JME-009-01 (2009).

[19] T. Plehn and M. Spannowsky, *Top tagging*, J. Phys. **G 39** (2012) 083001 [arXiv:1112.4441] [INSPIRE].

[20] CMS collaboration, *Search for anomalous $t\bar{t}$ production in the highly-boosted all-hadronic final state*, JHEP **09** (2012) 029 [arXiv:1204.2488] [INSPIRE].

[21] CMS collaboration, *Searches for new physics using the $t\bar{t}$ invariant mass distribution in pp collisions at $\sqrt{s} = 8$ TeV*, Phys. Rev. Lett. **111** (2013) 211804 [arXiv:1309.2030] [INSPIRE].

[22] ATLAS collaboration, *Search for resonances decaying into top-quark pairs using fully hadronic decays in pp collisions with ATLAS at $\sqrt{s} = 7$ TeV*, JHEP **01** (2013) 116 [arXiv:1211.2202] [INSPIRE].

[23] CMS collaboration, *Energy calibration and resolution of the CMS electromagnetic calorimeter in pp collisions at $\sqrt{s} = 7$ TeV*, 2013 JINST **8** P09009 [arXiv:1306.2016] [INSPIRE].

[24] CMS collaboration, *Description and performance of track and primary-vertex reconstruction with the CMS tracker*, 2014 JINST **9** P10009 [arXiv:1405.6569] [INSPIRE].

[25] CMS collaboration, *The CMS experiment at the CERN LHC*, 2008 JINST **3** S08004 [INSPIRE].

[26] M. Cacciari, G.P. Salam and G. Soyez, *The anti-k_t jet clustering algorithm*, JHEP **04** (2008) 063 [arXiv:0802.1189] [INSPIRE].

[27] M. Cacciari, G.P. Salam and G. Soyez, *FastJet user manual*, Eur. Phys. J. **C 72** (2012) 1896 [arXiv:1111.6097] [INSPIRE].

[28] M. Czakon, P. Fiedler and A. Mitov, *Total top-quark pair-production cross section at hadron colliders through $O(\alpha_S^4)$*, Phys. Rev. Lett. **110** (2013) 252004 [arXiv:1303.6254] [INSPIRE].

JHEP06(2015)080

[29] M. Czakon and A. Mitov, *Top++: a program for the calculation of the top-pair cross-section at hadron colliders*, Comput. Phys. Commun. **185** (2014) 2930 [arXiv:1112.5675] [INSPIRE].

[30] LHC Higgs Cross Section Working Group collaboration, S. Heinemeyer et al., *Handbook of LHC Higgs cross sections: 3. Higgs properties*, arXiv:1307.1347 [INSPIRE].

[31] P. Nason, *A new method for combining NLO QCD with shower Monte Carlo algorithms*, JHEP **11** (2004) 040 [hep-ph/0409146] [INSPIRE].

[32] S. Frixione, P. Nason and C. Oleari, *Matching NLO QCD computations with parton shower simulations: the POWHEG method*, JHEP **11** (2007) 070 [arXiv:0709.2092] [INSPIRE].

[33] S. Alioli, P. Nason, C. Oleari and E. Re, *A general framework for implementing NLO calculations in shower Monte Carlo programs: the POWHEG BOX*, JHEP **06** (2010) 043 [arXiv:1002.2581] [INSPIRE].

[34] T. Sjöstrand, S. Mrenna and P.Z. Skands, *PYTHIA 6.4 physics and manual*, JHEP **05** (2006) 026 [hep-ph/0603175] [INSPIRE].

[35] J. Alwall, M. Herquet, F. Maltoni, O. Mattelaer and T. Stelzer, *MadGraph 5: going beyond*, JHEP **06** (2011) 128 [arXiv:1106.0522] [INSPIRE].

[36] J. Pumplin et al., *New generation of parton distributions with uncertainties from global QCD analysis*, JHEP **07** (2002) 012 [hep-ph/0201195] [INSPIRE].

[37] R. Field, *Early LHC underlying event data-findings and surprises*, in 22nd *Hadron Collider Physics Symposium (HCP2010)*, W. Trischuk ed., Toronto University, Toronto (2010), arXiv:1010.3558 [INSPIRE].

[38] K. Rose, *Deterministic annealing for clustering, compression, classification, regression and related optimisation problems*, IEEE Proc. **86** (1998) 2210.

[39] W. Waltenberger, R. Früwirth, and P. Vanlaer, *Adaptive vertex fitting*, J. Phys. **G 34** (2007) N343.

[40] CMS collaboration, *Particle-flow event reconstruction in CMS and performance for jets, taus and MET*, CMS-PAS-PFT-09-001 (2009).

[41] CMS collaboration, *Commissioning of the particle-flow event reconstruction with the first LHC collisions recorded in the CMS detector*, CMS-PAS-PFT-10-001 (2010).

[42] Y.L. Dokshitzer, G.D. Leder, S. Moretti and B.R. Webber, *Better jet clustering algorithms*, JHEP **08** (1997) 001 [hep-ph/9707323] [INSPIRE].

[43] CMS collaboration, *Determination of jet energy calibration and transverse momentum resolution in CMS*, 2011 JINST **6** P11002 [arXiv:1107.4277] [INSPIRE].

[44] M. Cacciari, G.P. Salam and G. Soyez, *The catchment area of jets*, JHEP **04** (2008) 005 [arXiv:0802.1188] [INSPIRE].

[45] CMS collaboration, *Identification of b-quark jets with the CMS experiment*, 2013 JINST **8** P04013 [arXiv:1211.4462] [INSPIRE].

[46] S.D. Ellis, C.K. Vermilion and J.R. Walsh, *Techniques for improved heavy particle searches with jet substructure*, Phys. Rev. **D 80** (2009) 051501 [arXiv:0903.5081] [INSPIRE].

[47] D. Krohn, J. Thaler and L.-T. Wang, *Jet trimming*, JHEP **02** (2010) 084 [arXiv:0912.1342] [INSPIRE].

[48] CMS collaboration, *Boosted top jet tagging at CMS*, CMS-PAS-JME-13-007 (2013).

[49] CMS collaboration, *Performance of b tagging at $\sqrt{s} = 8$ TeV in multijet, ttbar and boosted topology events*, CMS-PAS-BTV-13-001 (2013).

[50] CMS Collaboration, *CMS luminosity based on pixel cluster counting — Summer 2013 update*, CMS-PAS-LUM-13-001 (2013).

[51] CMS collaboration, *Measurement of differential top-quark pair production cross sections in pp colisions at $\sqrt{s} = 7$ TeV*, Eur. Phys. J. **C 73** (2013) 2339 [arXiv:1211.2220] [INSPIRE].

[52] A. O'Hagan and J. Foster, *Kendalls advanced theory of statistic 2B: bayesian inference*, Wiley, U.S.A. (2010).

[53] J. Ott, http://www.theta-framework.org/.

The CMS collaboration

Yerevan Physics Institute, Yerevan, Armenia

V. Khachatryan, A.M. Sirunyan, A. Tumasyan

Institut für Hochenergiephysik der OeAW, Wien, Austria

W. Adam, T. Bergauer, M. Dragicevic, J. Erö, M. Friedl, R. Frühwirth[1], V.M. Ghete, C. Hartl, N. Hörmann, J. Hrubec, M. Jeitler[1], W. Kiesenhofer, V. Knünz, M. Krammer[1], I. Krätschmer, D. Liko, I. Mikulec, D. Rabady[2], B. Rahbaran, H. Rohringer, R. Schöfbeck, J. Strauss, W. Treberer-Treberspurg, W. Waltenberger, C.-E. Wulz[1]

National Centre for Particle and High Energy Physics, Minsk, Belarus

V. Mossolov, N. Shumeiko, J. Suarez Gonzalez

Universiteit Antwerpen, Antwerpen, Belgium

S. Alderweireldt, S. Bansal, T. Cornelis, E.A. De Wolf, X. Janssen, A. Knutsson, J. Lauwers, S. Luyckx, S. Ochesanu, R. Rougny, M. Van De Klundert, H. Van Haevermaet, P. Van Mechelen, N. Van Remortel, A. Van Spilbeeck

Vrije Universiteit Brussel, Brussel, Belgium

F. Blekman, S. Blyweert, J. D'Hondt, N. Daci, N. Heracleous, J. Keaveney, S. Lowette, M. Maes, A. Olbrechts, Q. Python, D. Strom, S. Tavernier, W. Van Doninck, P. Van Mulders, G.P. Van Onsem, I. Villella

Université Libre de Bruxelles, Bruxelles, Belgium

C. Caillol, B. Clerbaux, G. De Lentdecker, D. Dobur, L. Favart, A.P.R. Gay, A. Grebenyuk, A. Léonard, A. Mohammadi, L. Perniè[2], A. Randle-conde, T. Reis, T. Seva, L. Thomas, C. Vander Velde, P. Vanlaer, J. Wang, F. Zenoni

Ghent University, Ghent, Belgium

V. Adler, K. Beernaert, L. Benucci, A. Cimmino, S. Costantini, S. Crucy, S. Dildick, A. Fagot, G. Garcia, J. Mccartin, A.A. Ocampo Rios, D. Poyraz, D. Ryckbosch, S. Salva Diblen, M. Sigamani, N. Strobbe, F. Thyssen, M. Tytgat, E. Yazgan, N. Zaganidis

Université Catholique de Louvain, Louvain-la-Neuve, Belgium

S. Basegmez, C. Beluffi[3], G. Bruno, R. Castello, A. Caudron, L. Ceard, G.G. Da Silveira, C. Delaere, T. du Pree, D. Favart, L. Forthomme, A. Giammanco[4], J. Hollar, A. Jafari, P. Jez, M. Komm, V. Lemaitre, C. Nuttens, L. Perrini, A. Pin, K. Piotrzkowski, A. Popov[5], L. Quertenmont, M. Selvaggi, M. Vidal Marono, J.M. Vizan Garcia

Université de Mons, Mons, Belgium

N. Beliy, T. Caebergs, E. Daubie, G.H. Hammad

Centro Brasileiro de Pesquisas Fisicas, Rio de Janeiro, Brazil

W.L. Aldá Júnior, G.A. Alves, L. Brito, M. Correa Martins Junior, T. Dos Reis Martins, J. Molina, C. Mora Herrera, M.E. Pol, P. Rebello Teles

JHEP06(2015)080

Universidade do Estado do Rio de Janeiro, Rio de Janeiro, Brazil

W. Carvalho, J. Chinellato[6], A. Custódio, E.M. Da Costa, D. De Jesus Damiao, C. De Oliveira Martins, S. Fonseca De Souza, H. Malbouisson, D. Matos Figueiredo, L. Mundim, H. Nogima, W.L. Prado Da Silva, J. Santaolalla, A. Santoro, A. Sznajder, E.J. Tonelli Manganote[6], A. Vilela Pereira

Universidade Estadual Paulista [a], Universidade Federal do ABC [b], São Paulo, Brazil

C.A. Bernardes[b], S. Dogra[a], T.R. Fernandez Perez Tomei[a], E.M. Gregores[b], P.G. Mercadante[b], S.F. Novaes[a], Sandra S. Padula[a]

Institute for Nuclear Research and Nuclear Energy, Sofia, Bulgaria

A. Aleksandrov, V. Genchev[2], R. Hadjiiska, P. Iaydjiev, A. Marinov, S. Piperov, M. Rodozov, S. Stoykova, G. Sultanov, M. Vutova

University of Sofia, Sofia, Bulgaria

A. Dimitrov, I. Glushkov, L. Litov, B. Pavlov, P. Petkov

Institute of High Energy Physics, Beijing, China

J.G. Bian, G.M. Chen, H.S. Chen, M. Chen, T. Cheng, R. Du, C.H. Jiang, R. Plestina[7], F. Romeo, J. Tao, Z. Wang

State Key Laboratory of Nuclear Physics and Technology, Peking University, Beijing, China

C. Asawatangtrakuldee, Y. Ban, S. Liu, Y. Mao, S.J. Qian, D. Wang, Z. Xu, L. Zhang, W. Zou

Universidad de Los Andes, Bogota, Colombia

C. Avila, A. Cabrera, L.F. Chaparro Sierra, C. Florez, J.P. Gomez, B. Gomez Moreno, J.C. Sanabria

University of Split, Faculty of Electrical Engineering, Mechanical Engineering and Naval Architecture, Split, Croatia

N. Godinovic, D. Lelas, D. Polic, I. Puljak

University of Split, Faculty of Science, Split, Croatia

Z. Antunovic, M. Kovac

Institute Rudjer Boskovic, Zagreb, Croatia

V. Brigljevic, K. Kadija, J. Luetic, D. Mekterovic, L. Sudic

University of Cyprus, Nicosia, Cyprus

A. Attikis, G. Mavromanolakis, J. Mousa, C. Nicolaou, F. Ptochos, P.A. Razis, H. Rykaczewski

Charles University, Prague, Czech Republic

M. Bodlak, M. Finger, M. Finger Jr.[8]

JHEP06(2015)080

Academy of Scientific Research and Technology of the Arab Republic of Egypt, Egyptian Network of High Energy Physics, Cairo, Egypt
Y. Assran[9], A. Ellithi Kamel[10], M.A. Mahmoud[11], A. Radi[12,13]

National Institute of Chemical Physics and Biophysics, Tallinn, Estonia
M. Kadastik, M. Murumaa, M. Raidal, A. Tiko

Department of Physics, University of Helsinki, Helsinki, Finland
P. Eerola, M. Voutilainen

Helsinki Institute of Physics, Helsinki, Finland
J. Härkönen, V. Karimäki, R. Kinnunen, M.J. Kortelainen, T. Lampén, K. Lassila-Perini, S. Lehti, T. Lindén, P. Luukka, T. Mäenpää, T. Peltola, E. Tuominen, J. Tuominiemi, E. Tuovinen, L. Wendland

Lappeenranta University of Technology, Lappeenranta, Finland
J. Talvitie, T. Tuuva

DSM/IRFU, CEA/Saclay, Gif-sur-Yvette, France
M. Besancon, F. Couderc, M. Dejardin, D. Denegri, B. Fabbro, J.L. Faure, C. Favaro, F. Ferri, S. Ganjour, A. Givernaud, P. Gras, G. Hamel de Monchenault, P. Jarry, E. Locci, J. Malcles, J. Rander, A. Rosowsky, M. Titov

Laboratoire Leprince-Ringuet, Ecole Polytechnique, IN2P3-CNRS, Palaiseau, France
S. Baffioni, F. Beaudette, P. Busson, E. Chapon, C. Charlot, T. Dahms, M. Dalchenko, L. Dobrzynski, N. Filipovic, A. Florent, R. Granier de Cassagnac, L. Mastrolorenzo, P. Miné, I.N. Naranjo, M. Nguyen, C. Ochando, G. Ortona, P. Paganini, S. Regnard, R. Salerno, J.B. Sauvan, Y. Sirois, C. Veelken, Y. Yilmaz, A. Zabi

Institut Pluridisciplinaire Hubert Curien, Université de Strasbourg, Université de Haute Alsace Mulhouse, CNRS/IN2P3, Strasbourg, France
J.-L. Agram[14], J. Andrea, A. Aubin, D. Bloch, J.-M. Brom, E.C. Chabert, C. Collard, E. Conte[14], J.-C. Fontaine[14], D. Gelé, U. Goerlach, C. Goetzmann, A.-C. Le Bihan, K. Skovpen, P. Van Hove

Centre de Calcul de l'Institut National de Physique Nucleaire et de Physique des Particules, CNRS/IN2P3, Villeurbanne, France
S. Gadrat

Université de Lyon, Université Claude Bernard Lyon 1, CNRS-IN2P3, Institut de Physique Nucléaire de Lyon, Villeurbanne, France
S. Beauceron, N. Beaupere, C. Bernet[7], G. Boudoul[2], E. Bouvier, S. Brochet, C.A. Carrillo Montoya, J. Chasserat, R. Chierici, D. Contardo[2], B. Courbon, P. Depasse, H. El Mamouni, J. Fan, J. Fay, S. Gascon, M. Gouzevitch, B. Ille, T. Kurca, M. Lethuillier, L. Mirabito, A.L. Pequegnot, S. Perries, J.D. Ruiz Alvarez, D. Sabes, L. Sgandurra, V. Sordini, M. Vander Donckt, P. Verdier, S. Viret, H. Xiao

Institute of High Energy Physics and Informatization, Tbilisi State University, Tbilisi, Georgia

Z. Tsamalaidze[8]

RWTH Aachen University, I. Physikalisches Institut, Aachen, Germany

C. Autermann, S. Beranek, M. Bontenackels, M. Edelhoff, L. Feld, A. Heister, K. Klein, M. Lipinski, A. Ostapchuk, M. Preuten, F. Raupach, J. Sammet, S. Schael, J.F. Schulte, H. Weber, B. Wittmer, V. Zhukov[5]

RWTH Aachen University, III. Physikalisches Institut A, Aachen, Germany

M. Ata, M. Brodski, E. Dietz-Laursonn, D. Duchardt, M. Erdmann, R. Fischer, A. Güth, T. Hebbeker, C. Heidemann, K. Hoepfner, D. Klingebiel, S. Knutzen, P. Kreuzer, M. Merschmeyer, A. Meyer, P. Millet, M. Olschewski, K. Padeken, P. Papacz, H. Reithler, S.A. Schmitz, L. Sonnenschein, D. Teyssier, S. Thüer, M. Weber

RWTH Aachen University, III. Physikalisches Institut B, Aachen, Germany

V. Cherepanov, Y. Erdogan, G. Flügge, H. Geenen, M. Geisler, W. Haj Ahmad, F. Hoehle, B. Kargoll, T. Kress, Y. Kuessel, A. Künsken, J. Lingemann[2], A. Nowack, I.M. Nugent, O. Pooth, A. Stahl

Deutsches Elektronen-Synchrotron, Hamburg, Germany

M. Aldaya Martin, I. Asin, N. Bartosik, J. Behr, U. Behrens, A.J. Bell, A. Bethani, K. Borras, A. Burgmeier, A. Cakir, L. Calligaris, A. Campbell, S. Choudhury, F. Costanza, C. Diez Pardos, G. Dolinska, S. Dooling, T. Dorland, G. Eckerlin, D. Eckstein, T. Eichhorn, G. Flucke, J. Garay Garcia, A. Geiser, A. Gizhko, P. Gunnellini, J. Hauk, M. Hempel[15], H. Jung, A. Kalogeropoulos, O. Karacheban[15], M. Kasemann, P. Katsas, J. Kieseler, C. Kleinwort, I. Korol, D. Krücker, W. Lange, J. Leonard, K. Lipka, A. Lobanov, W. Lohmann[15], B. Lutz, R. Mankel, I. Marfin[15], I.-A. Melzer-Pellmann, A.B. Meyer, G. Mittag, J. Mnich, A. Mussgiller, S. Naumann-Emme, A. Nayak, E. Ntomari, H. Perrey, D. Pitzl, R. Placakyte, A. Raspereza, P.M. Ribeiro Cipriano, B. Roland, E. Ron, M.Ö. Sahin, J. Salfeld-Nebgen, P. Saxena, T. Schoerner-Sadenius, M. Schröder, C. Seitz, S. Spannagel, A.D.R. Vargas Trevino, R. Walsh, C. Wissing

University of Hamburg, Hamburg, Germany

V. Blobel, M. Centis Vignali, A.R. Draeger, J. Erfle, E. Garutti, K. Goebel, M. Görner, J. Haller, M. Hoffmann, R.S. Höing, A. Junkes, H. Kirschenmann, R. Klanner, R. Kogler, T. Lapsien, T. Lenz, I. Marchesini, D. Marconi, J. Ott, T. Peiffer, A. Perieanu, N. Pietsch, J. Poehlsen, T. Poehlsen, D. Rathjens, C. Sander, H. Schettler, P. Schleper, E. Schlieckau, A. Schmidt, M. Seidel, V. Sola, H. Stadie, G. Steinbrück, D. Troendle, E. Usai, L. Vanelderen, A. Vanhoefer

Institut für Experimentelle Kernphysik, Karlsruhe, Germany

C. Barth, C. Baus, J. Berger, C. Böser, E. Butz, T. Chwalek, W. De Boer, A. Descroix, A. Dierlamm, M. Feindt, F. Frensch, M. Giffels, A. Gilbert, F. Hartmann[2], T. Hauth, U. Husemann, I. Katkov[5], A. Kornmayer[2], P. Lobelle Pardo, M.U. Mozer, T. Müller, Th. Müller, A. Nürnberg, G. Quast, K. Rabbertz, S. Röcker, H.J. Simonis, F.M. Stober, R. Ulrich, J. Wagner-Kuhr, S. Wayand, T. Weiler, R. Wolf

Institute of Nuclear and Particle Physics (INPP), NCSR Demokritos, Aghia Paraskevi, Greece

G. Anagnostou, G. Daskalakis, T. Geralis, V.A. Giakoumopoulou, A. Kyriakis, D. Loukas, A. Markou, C. Markou, A. Psallidas, I. Topsis-Giotis

University of Athens, Athens, Greece

A. Agapitos, S. Kesisoglou, A. Panagiotou, N. Saoulidou, E. Stiliaris

University of Ioánnina, Ioánnina, Greece

X. Aslanoglou, I. Evangelou, G. Flouris, C. Foudas, P. Kokkas, N. Manthos, I. Papadopoulos, E. Paradas, J. Strologas

Wigner Research Centre for Physics, Budapest, Hungary

G. Bencze, C. Hajdu, P. Hidas, D. Horvath[16], F. Sikler, V. Veszpremi, G. Vesztergombi[17], A.J. Zsigmond

Institute of Nuclear Research ATOMKI, Debrecen, Hungary

N. Beni, S. Czellar, J. Karancsi[18], J. Molnar, J. Palinkas, Z. Szillasi

University of Debrecen, Debrecen, Hungary

A. Makovec, P. Raics, Z.L. Trocsanyi, B. Ujvari

National Institute of Science Education and Research, Bhubaneswar, India

S.K. Swain

Panjab University, Chandigarh, India

S.B. Beri, V. Bhatnagar, R. Gupta, U.Bhawandeep, A.K. Kalsi, M. Kaur, R. Kumar, M. Mittal, N. Nishu, J.B. Singh

University of Delhi, Delhi, India

Ashok Kumar, Arun Kumar, S. Ahuja, A. Bhardwaj, B.C. Choudhary, A. Kumar, S. Malhotra, M. Naimuddin, K. Ranjan, V. Sharma

Saha Institute of Nuclear Physics, Kolkata, India

S. Banerjee, S. Bhattacharya, K. Chatterjee, S. Dutta, B. Gomber, Sa. Jain, Sh. Jain, R. Khurana, A. Modak, S. Mukherjee, D. Roy, S. Sarkar, M. Sharan

Bhabha Atomic Research Centre, Mumbai, India

A. Abdulsalam, D. Dutta, V. Kumar, A.K. Mohanty[2], L.M. Pant, P. Shukla, A. Topkar

Tata Institute of Fundamental Research, Mumbai, India

T. Aziz, S. Banerjee, S. Bhowmik[19], R.M. Chatterjee, R.K. Dewanjee, S. Dugad, S. Ganguly, S. Ghosh, M. Guchait, A. Gurtu[20], G. Kole, S. Kumar, M. Maity[19], G. Majumder, K. Mazumdar, G.B. Mohanty, B. Parida, K. Sudhakar, N. Wickramage[21]

Indian Institute of Science Education and Research (IISER), Pune, India

S. Sharma

JHEP06(2015)080

Institute for Research in Fundamental Sciences (IPM), Tehran, Iran

H. Bakhshiansohi, H. Behnamian, S.M. Etesami[22], A. Fahim[23], R. Goldouzian, M. Khakzad, M. Mohammadi Najafabadi, M. Naseri, S. Paktinat Mehdiabadi, F. Rezaei Hosseinabadi, B. Safarzadeh[24], M. Zeinali

University College Dublin, Dublin, Ireland

M. Felcini, M. Grunewald

INFN Sezione di Bari [a], Università di Bari [b], Politecnico di Bari [c], Bari, Italy

M. Abbrescia[a,b], C. Calabria[a,b], S.S. Chhibra[a,b], A. Colaleo[a], D. Creanza[a,c], L. Cristella[a,b], N. De Filippis[a,c], M. De Palma[a,b], L. Fiore[a], G. Iaselli[a,c], G. Maggi[a,c], M. Maggi[a], S. My[a,c], S. Nuzzo[a,b], A. Pompili[a,b], G. Pugliese[a,c], R. Radogna[a,b,2], G. Selvaggi[a,b], A. Sharma[a], L. Silvestris[a,2], R. Venditti[a,b], P. Verwilligen[a]

INFN Sezione di Bologna [a], Università di Bologna [b], Bologna, Italy

G. Abbiendi[a], A.C. Benvenuti[a], D. Bonacorsi[a,b], S. Braibant-Giacomelli[a,b], L. Brigliadori[a,b], R. Campanini[a,b], P. Capiluppi[a,b], A. Castro[a,b], F.R. Cavallo[a], G. Codispoti[a,b], M. Cuffiani[a,b], G.M. Dallavalle[a], F. Fabbri[a], A. Fanfani[a,b], D. Fasanella[a,b], P. Giacomelli[a], C. Grandi[a], L. Guiducci[a,b], S. Marcellini[a], G. Masetti[a], A. Montanari[a], F.L. Navarria[a,b], A. Perrotta[a], A.M. Rossi[a,b], T. Rovelli[a,b], G.P. Siroli[a,b], N. Tosi[a,b], R. Travaglini[a,b]

INFN Sezione di Catania [a], Università di Catania [b], CSFNSM [c], Catania, Italy

S. Albergo[a,b], G. Cappello[a], M. Chiorboli[a,b], S. Costa[a,b], F. Giordano[a,2], R. Potenza[a,b], A. Tricomi[a,b], C. Tuve[a,b]

INFN Sezione di Firenze [a], Università di Firenze [b], Firenze, Italy

G. Barbagli[a], V. Ciulli[a,b], C. Civinini[a], R. D'Alessandro[a,b], E. Focardi[a,b], E. Gallo[a], S. Gonzi[a,b], V. Gori[a,b], P. Lenzi[a,b], M. Meschini[a], S. Paoletti[a], G. Sguazzoni[a], A. Tropiano[a,b]

INFN Laboratori Nazionali di Frascati, Frascati, Italy

L. Benussi, S. Bianco, F. Fabbri, D. Piccolo

INFN Sezione di Genova [a], Università di Genova [b], Genova, Italy

R. Ferretti[a,b], F. Ferro[a], M. Lo Vetere[a,b], E. Robutti[a], S. Tosi[a,b]

INFN Sezione di Milano-Bicocca [a], Università di Milano-Bicocca [b], Milano, Italy

M.E. Dinardo[a,b], S. Fiorendi[a,b], S. Gennai[a,2], R. Gerosa[a,b,2], A. Ghezzi[a,b], P. Govoni[a,b], M.T. Lucchini[a,b,2], S. Malvezzi[a], R.A. Manzoni[a,b], A. Martelli[a,b], B. Marzocchi[a,b,2], D. Menasce[a], L. Moroni[a], M. Paganoni[a,b], D. Pedrini[a], S. Ragazzi[a,b], N. Redaelli[a], T. Tabarelli de Fatis[a,b]

JHEP06(2015)080

INFN Sezione di Napoli [a], Università di Napoli 'Federico II' [b], Napoli, Italy, Università della Basilicata [c], Potenza, Italy, Università G. Marconi [d], Roma, Italy

S. Buontempo[a], N. Cavallo[a,c], S. Di Guida[a,d,2], F. Fabozzi[a,c], A.O.M. Iorio[a,b], L. Lista[a], S. Meola[a,d,2], M. Merola[a], P. Paolucci[a,2]

INFN Sezione di Padova [a], Università di Padova [b], Padova, Italy, Università di Trento [c], Trento, Italy

P. Azzi[a], N. Bacchetta[a], D. Bisello[a,b], A. Branca[a,b], R. Carlin[a,b], P. Checchia[a], M. Dall'Osso[a,b], T. Dorigo[a], U. Dosselli[a], F. Gasparini[a,b], U. Gasparini[a,b], A. Gozzelino[a], K. Kanishchev[a,c], S. Lacaprara[a], M. Margoni[a,b], A.T. Meneguzzo[a,b], J. Pazzini[a,b], N. Pozzobon[a,b], P. Ronchese[a,b], F. Simonetto[a,b], E. Torassa[a], M. Tosi[a,b], P. Zotto[a,b], A. Zucchetta[a,b], G. Zumerle[a,b]

INFN Sezione di Pavia [a], Università di Pavia [b], Pavia, Italy

M. Gabusi[a,b], S.P. Ratti[a,b], V. Re[a], C. Riccardi[a,b], P. Salvini[a], P. Vitulo[a,b]

INFN Sezione di Perugia [a], Università di Perugia [b], Perugia, Italy

M. Biasini[a,b], G.M. Bilei[a], D. Ciangottini[a,b,2], L. Fanò[a,b], P. Lariccia[a,b], G. Mantovani[a,b], M. Menichelli[a], A. Saha[a], A. Santocchia[a,b], A. Spiezia[a,b,2]

INFN Sezione di Pisa [a], Università di Pisa [b], Scuola Normale Superiore di Pisa [c], Pisa, Italy

K. Androsov[a,25], P. Azzurri[a], G. Bagliesi[a], J. Bernardini[a], T. Boccali[a], G. Broccolo[a,c], R. Castaldi[a], M.A. Ciocci[a,25], R. Dell'Orso[a], S. Donato[a,c,2], G. Fedi, F. Fiori[a,c], L. Foà[a,c], A. Giassi[a], M.T. Grippo[a,25], F. Ligabue[a,c], T. Lomtadze[a], L. Martini[a,b], A. Messineo[a,b], C.S. Moon[a,26], F. Palla[a,2], A. Rizzi[a,b], A. Savoy-Navarro[a,27], A.T. Serban[a], P. Spagnolo[a], P. Squillacioti[a,25], R. Tenchini[a], G. Tonelli[a,b], A. Venturi[a], P.G. Verdini[a], C. Vernieri[a,c]

INFN Sezione di Roma [a], Università di Roma [b], Roma, Italy

L. Barone[a,b], F. Cavallari[a], G. D'imperio[a,b], D. Del Re[a,b], M. Diemoz[a], C. Jorda[a], E. Longo[a,b], F. Margaroli[a,b], P. Meridiani[a], F. Micheli[a,b,2], G. Organtini[a,b], R. Paramatti[a], S. Rahatlou[a,b], C. Rovelli[a], F. Santanastasio[a,b], L. Soffi[a,b], P. Traczyk[a,b,2]

INFN Sezione di Torino [a], Università di Torino [b], Torino, Italy, Università del Piemonte Orientale [c], Novara, Italy

N. Amapane[a,b], R. Arcidiacono[a,c], S. Argiro[a,b], M. Arneodo[a,c], R. Bellan[a,b], C. Biino[a], N. Cartiglia[a], S. Casasso[a,b,2], M. Costa[a,b], R. Covarelli, A. Degano[a,b], N. Demaria[a], L. Finco[a,b,2], C. Mariotti[a], S. Maselli[a], E. Migliore[a,b], V. Monaco[a,b], M. Musich[a], M.M. Obertino[a,c], L. Pacher[a,b], N. Pastrone[a], M. Pelliccioni[a], G.L. Pinna Angioni[a,b], A. Potenza[a,b], A. Romero[a,b], M. Ruspa[a,c], R. Sacchi[a,b], A. Solano[a,b], A. Staiano[a], U. Tamponi[a]

INFN Sezione di Trieste [a], Università di Trieste [b], Trieste, Italy

S. Belforte[a], V. Candelise[a,b,2], M. Casarsa[a], F. Cossutti[a], G. Della Ricca[a,b], B. Gobbo[a], C. La Licata[a,b], M. Marone[a,b], A. Schizzi[a,b], T. Umer[a,b], A. Zanetti[a]

JHEP06(2015)080

Kangwon National University, Chunchon, Korea
S. Chang, A. Kropivnitskaya, S.K. Nam

Kyungpook National University, Daegu, Korea
D.H. Kim, G.N. Kim, M.S. Kim, D.J. Kong, S. Lee, Y.D. Oh, H. Park, A. Sakharov, D.C. Son

Chonbuk National University, Jeonju, Korea
T.J. Kim, M.S. Ryu

Chonnam National University, Institute for Universe and Elementary Particles, Kwangju, Korea
J.Y. Kim, D.H. Moon, S. Song

Korea University, Seoul, Korea
S. Choi, D. Gyun, B. Hong, M. Jo, H. Kim, Y. Kim, B. Lee, K.S. Lee, S.K. Park, Y. Roh

Seoul National University, Seoul, Korea
H.D. Yoo

University of Seoul, Seoul, Korea
M. Choi, J.H. Kim, I.C. Park, G. Ryu

Sungkyunkwan University, Suwon, Korea
Y. Choi, Y.K. Choi, J. Goh, D. Kim, E. Kwon, J. Lee, I. Yu

Vilnius University, Vilnius, Lithuania
A. Juodagalvis

National Centre for Particle Physics, Universiti Malaya, Kuala Lumpur, Malaysia
J.R. Komaragiri, M.A.B. Md Ali

Centro de Investigacion y de Estudios Avanzados del IPN, Mexico City, Mexico
E. Casimiro Linares, H. Castilla-Valdez, E. De La Cruz-Burelo, I. Heredia-de La Cruz, A. Hernandez-Almada, R. Lopez-Fernandez, A. Sanchez-Hernandez

Universidad Iberoamericana, Mexico City, Mexico
S. Carrillo Moreno, F. Vazquez Valencia

Benemerita Universidad Autonoma de Puebla, Puebla, Mexico
I. Pedraza, H.A. Salazar Ibarguen

Universidad Autónoma de San Luis Potosí, San Luis Potosí, Mexico
A. Morelos Pineda

University of Auckland, Auckland, New Zealand
D. Krofcheck

University of Canterbury, Christchurch, New Zealand
P.H. Butler, S. Reucroft

JHEP06(2015)080

National Centre for Physics, Quaid-I-Azam University, Islamabad, Pakistan
A. Ahmad, M. Ahmad, Q. Hassan, H.R. Hoorani, W.A. Khan, T. Khurshid, M. Shoaib

National Centre for Nuclear Research, Swierk, Poland
H. Bialkowska, M. Bluj, B. Boimska, T. Frueboes, M. Górski, M. Kazana, K. Nawrocki, K. Romanowska-Rybinska, M. Szleper, P. Zalewski

Institute of Experimental Physics, Faculty of Physics, University of Warsaw, Warsaw, Poland
G. Brona, K. Bunkowski, M. Cwiok, W. Dominik, K. Doroba, A. Kalinowski, M. Konecki, J. Krolikowski, M. Misiura, M. Olszewski

Laboratório de Instrumentação e Física Experimental de Partículas, Lisboa, Portugal
P. Bargassa, C. Beirão Da Cruz E Silva, P. Faccioli, P.G. Ferreira Parracho, M. Gallinaro, L. Lloret Iglesias, F. Nguyen, J. Rodrigues Antunes, J. Seixas, J. Varela, P. Vischia

Joint Institute for Nuclear Research, Dubna, Russia
P. Bunin, I. Golutvin, I. Gorbunov, V. Karjavin, V. Konoplyanikov, G. Kozlov, A. Lanev, A. Malakhov, V. Matveev[28], P. Moisenz, V. Palichik, V. Perelygin, M. Savina, S. Shmatov, S. Shulha, N. Skatchkov, V. Smirnov, A. Zarubin

Petersburg Nuclear Physics Institute, Gatchina (St. Petersburg), Russia
V. Golovtsov, Y. Ivanov, V. Kim[29], E. Kuznetsova, P. Levchenko, V. Murzin, V. Oreshkin, I. Smirnov, V. Sulimov, L. Uvarov, S. Vavilov, A. Vorobyev, An. Vorobyev

Institute for Nuclear Research, Moscow, Russia
Yu. Andreev, A. Dermenev, S. Gninenko, N. Golubev, M. Kirsanov, N. Krasnikov, A. Pashenkov, D. Tlisov, A. Toropin

Institute for Theoretical and Experimental Physics, Moscow, Russia
V. Epshteyn, V. Gavrilov, N. Lychkovskaya, V. Popov, I. Pozdnyakov, G. Safronov, S. Semenov, A. Spiridonov, V. Stolin, E. Vlasov, A. Zhokin

P.N. Lebedev Physical Institute, Moscow, Russia
V. Andreev, M. Azarkin[30], I. Dremin[30], M. Kirakosyan, A. Leonidov[30], G. Mesyats, S.V. Rusakov, A. Vinogradov

Skobeltsyn Institute of Nuclear Physics, Lomonosov Moscow State University, Moscow, Russia
A. Belyaev, E. Boos, V. Bunichev, M. Dubinin[31], L. Dudko, A. Ershov, A. Gribushin, V. Klyukhin, O. Kodolova, I. Lokhtin, S. Obraztsov, V. Savrin, A. Snigirev

State Research Center of Russian Federation, Institute for High Energy Physics, Protvino, Russia
I. Azhgirey, I. Bayshev, S. Bitioukov, V. Kachanov, A. Kalinin, D. Konstantinov, V. Krychkine, V. Petrov, R. Ryutin, A. Sobol, L. Tourtchanovitch, S. Troshin, N. Tyurin, A. Uzunian, A. Volkov

JHEP06(2015)080

University of Belgrade, Faculty of Physics and Vinca Institute of Nuclear Sciences, Belgrade, Serbia

P. Adzic[32], M. Ekmedzic, J. Milosevic, V. Rekovic

Centro de Investigaciones Energéticas Medioambientales y Tecnológicas (CIEMAT), Madrid, Spain

J. Alcaraz Maestre, C. Battilana, E. Calvo, M. Cerrada, M. Chamizo Llatas, N. Colino, B. De La Cruz, A. Delgado Peris, D. Domínguez Vázquez, A. Escalante Del Valle, C. Fernandez Bedoya, J.P. Fernández Ramos, J. Flix, M.C. Fouz, P. Garcia-Abia, O. Gonzalez Lopez, S. Goy Lopez, J.M. Hernandez, M.I. Josa, E. Navarro De Martino, A. Pérez-Calero Yzquierdo, J. Puerta Pelayo, A. Quintario Olmeda, I. Redondo, L. Romero, M.S. Soares

Universidad Autónoma de Madrid, Madrid, Spain

C. Albajar, J.F. de Trocóniz, M. Missiroli, D. Moran

Universidad de Oviedo, Oviedo, Spain

H. Brun, J. Cuevas, J. Fernandez Menendez, S. Folgueras, I. Gonzalez Caballero

Instituto de Física de Cantabria (IFCA), CSIC-Universidad de Cantabria, Santander, Spain

J.A. Brochero Cifuentes, I.J. Cabrillo, A. Calderon, J. Duarte Campderros, M. Fernandez, G. Gomez, A. Graziano, A. Lopez Virto, J. Marco, R. Marco, C. Martinez Rivero, F. Matorras, F.J. Munoz Sanchez, J. Piedra Gomez, T. Rodrigo, A.Y. Rodríguez-Marrero, A. Ruiz-Jimeno, L. Scodellaro, I. Vila, R. Vilar Cortabitarte

CERN, European Organization for Nuclear Research, Geneva, Switzerland

D. Abbaneo, E. Auffray, G. Auzinger, M. Bachtis, P. Baillon, A.H. Ball, D. Barney, A. Benaglia, J. Bendavid, L. Benhabib, J.F. Benitez, P. Bloch, A. Bocci, A. Bonato, O. Bondu, C. Botta, H. Breuker, T. Camporesi, G. Cerminara, S. Colafranceschi[33], M. D'Alfonso, D. d'Enterria, A. Dabrowski, A. David, F. De Guio, A. De Roeck, S. De Visscher, E. Di Marco, M. Dobson, M. Dordevic, B. Dorney, N. Dupont-Sagorin, A. Elliott-Peisert, G. Franzoni, W. Funk, D. Gigi, K. Gill, D. Giordano, M. Girone, F. Glege, R. Guida, S. Gundacker, M. Guthoff, J. Hammer, M. Hansen, P. Harris, J. Hegeman, V. Innocente, P. Janot, K. Kousouris, K. Krajczar, P. Lecoq, C. Lourenço, N. Magini, L. Malgeri, M. Mannelli, J. Marrouche, L. Masetti, F. Meijers, S. Mersi, E. Meschi, F. Moortgat, S. Morovic, M. Mulders, L. Orsini, L. Pape, E. Perez, A. Petrilli, G. Petrucciani, A. Pfeiffer, M. Pimiä, D. Piparo, M. Plagge, A. Racz, G. Rolandi[34], M. Rovere, H. Sakulin, C. Schäfer, C. Schwick, A. Sharma, P. Siegrist, P. Silva, M. Simon, P. Sphicas[35], D. Spiga, J. Steggemann, B. Stieger, M. Stoye, Y. Takahashi, D. Treille, A. Tsirou, G.I. Veres[17], N. Wardle, H.K. Wöhri, H. Wollny, W.D. Zeuner

Paul Scherrer Institut, Villigen, Switzerland

W. Bertl, K. Deiters, W. Erdmann, R. Horisberger, Q. Ingram, H.C. Kaestli, D. Kotlinski, U. Langenegger, D. Renker, T. Rohe

JHEP06(2015)080

Institute for Particle Physics, ETH Zurich, Zurich, Switzerland

F. Bachmair, L. Bäni, L. Bianchini, M.A. Buchmann, B. Casal, N. Chanon, G. Dissertori, M. Dittmar, M. Donegà, M. Dünser, P. Eller, C. Grab, D. Hits, J. Hoss, W. Lustermann, B. Mangano, A.C. Marini, M. Marionneau, P. Martinez Ruiz del Arbol, M. Masciovecchio, D. Meister, N. Mohr, P. Musella, C. Nägeli[36], F. Nessi-Tedaldi, F. Pandolfi, F. Pauss, L. Perrozzi, M. Peruzzi, M. Quittnat, L. Rebane, M. Rossini, A. Starodumov[37], M. Takahashi, K. Theofilatos, R. Wallny, H.A. Weber

Universität Zürich, Zurich, Switzerland

C. Amsler[38], M.F. Canelli, V. Chiochia, A. De Cosa, A. Hinzmann, T. Hreus, B. Kilminster, C. Lange, J. Ngadiuba, D. Pinna, P. Robmann, F.J. Ronga, S. Taroni, M. Verzetti, Y. Yang

National Central University, Chung-Li, Taiwan

M. Cardaci, K.H. Chen, C. Ferro, C.M. Kuo, W. Lin, Y.J. Lu, R. Volpe, S.S. Yu

National Taiwan University (NTU), Taipei, Taiwan

P. Chang, Y.H. Chang, Y. Chao, K.F. Chen, P.H. Chen, C. Dietz, U. Grundler, W.-S. Hou, Y.F. Liu, R.-S. Lu, M. Miñano Moya, E. Petrakou, Y.M. Tzeng, R. Wilken

Chulalongkorn University, Faculty of Science, Department of Physics, Bangkok, Thailand

B. Asavapibhop, G. Singh, N. Srimanobhas, N. Suwonjandee

Cukurova University, Adana, Turkey

A. Adiguzel, M.N. Bakirci[39], S. Cerci[40], C. Dozen, I. Dumanoglu, E. Eskut, S. Girgis, G. Gokbulut, Y. Guler, E. Gurpinar, I. Hos, E.E. Kangal[41], A. Kayis Topaksu, G. Onengut[42], K. Ozdemir[43], S. Ozturk[39], A. Polatoz, D. Sunar Cerci[40], B. Tali[40], H. Topakli[39], M. Vergili, C. Zorbilmez

Middle East Technical University, Physics Department, Ankara, Turkey

I.V. Akin, B. Bilin, S. Bilmis, H. Gamsizkan[44], B. Isildak[45], G. Karapinar[46], K. Ocalan[47], S. Sekmen, U.E. Surat, M. Yalvac, M. Zeyrek

Bogazici University, Istanbul, Turkey

E.A. Albayrak[48], E. Gülmez, M. Kaya[49], O. Kaya[50], T. Yetkin[51]

Istanbul Technical University, Istanbul, Turkey

K. Cankocak, F.I. Vardarlı

National Scientific Center, Kharkov Institute of Physics and Technology, Kharkov, Ukraine

L. Levchuk, P. Sorokin

University of Bristol, Bristol, United Kingdom

J.J. Brooke, E. Clement, D. Cussans, H. Flacher, J. Goldstein, M. Grimes, G.P. Heath, H.F. Heath, J. Jacob, L. Kreczko, C. Lucas, Z. Meng, D.M. Newbold[52], S. Paramesvaran, A. Poll, T. Sakuma, S. Seif El Nasr-storey, S. Senkin, V.J. Smith

JHEP06(2015)080

Rutherford Appleton Laboratory, Didcot, United Kingdom

K.W. Bell, A. Belyaev[53], C. Brew, R.M. Brown, D.J.A. Cockerill, J.A. Coughlan, K. Harder, S. Harper, E. Olaiya, D. Petyt, C.H. Shepherd-Themistocleous, A. Thea, I.R. Tomalin, T. Williams, W.J. Womersley, S.D. Worm

Imperial College, London, United Kingdom

M. Baber, R. Bainbridge, O. Buchmuller, D. Burton, D. Colling, N. Cripps, P. Dauncey, G. Davies, M. Della Negra, P. Dunne, A. Elwood, W. Ferguson, J. Fulcher, D. Futyan, G. Hall, G. Iles, M. Jarvis, G. Karapostoli, M. Kenzie, R. Lane, R. Lucas[52], L. Lyons, A.-M. Magnan, S. Malik, B. Mathias, J. Nash, A. Nikitenko[37], J. Pela, M. Pesaresi, K. Petridis, D.M. Raymond, S. Rogerson, A. Rose, C. Seez, P. Sharp[†], A. Tapper, M. Vazquez Acosta, T. Virdee, S.C. Zenz

Brunel University, Uxbridge, United Kingdom

J.E. Cole, P.R. Hobson, A. Khan, P. Kyberd, D. Leggat, D. Leslie, I.D. Reid, P. Symonds, L. Teodorescu, M. Turner

Baylor University, Waco, U.S.A.

J. Dittmann, K. Hatakeyama, A. Kasmi, H. Liu, N. Pastika, T. Scarborough, Z. Wu

The University of Alabama, Tuscaloosa, U.S.A.

O. Charaf, S.I. Cooper, C. Henderson, P. Rumerio

Boston University, Boston, U.S.A.

A. Avetisyan, T. Bose, C. Fantasia, P. Lawson, C. Richardson, J. Rohlf, J. St. John, L. Sulak

Brown University, Providence, U.S.A.

J. Alimena, E. Berry, S. Bhattacharya, G. Christopher, D. Cutts, Z. Demiragli, N. Dhingra, A. Ferapontov, A. Garabedian, U. Heintz, G. Kukartsev, E. Laird, G. Landsberg, M. Luk, M. Narain, M. Segala, T. Sinthuprasith, T. Speer, J. Swanson

University of California, Davis, Davis, U.S.A.

R. Breedon, G. Breto, M. Calderon De La Barca Sanchez, S. Chauhan, M. Chertok, J. Conway, R. Conway, P.T. Cox, R. Erbacher, M. Gardner, W. Ko, R. Lander, M. Mulhearn, D. Pellett, J. Pilot, F. Ricci-Tam, S. Shalhout, J. Smith, M. Squires, D. Stolp, M. Tripathi, S. Wilbur, R. Yohay

University of California, Los Angeles, U.S.A.

R. Cousins, P. Everaerts, C. Farrell, J. Hauser, M. Ignatenko, G. Rakness, E. Takasugi, V. Valuev, M. Weber

University of California, Riverside, Riverside, U.S.A.

K. Burt, R. Clare, J. Ellison, J.W. Gary, G. Hanson, J. Heilman, M. Ivova Rikova, P. Jandir, E. Kennedy, F. Lacroix, O.R. Long, A. Luthra, M. Malberti, M. Olmedo Negrete, A. Shrinivas, S. Sumowidagdo, S. Wimpenny

JHEP06(2015)080

University of California, San Diego, La Jolla, U.S.A.
J.G. Branson, G.B. Cerati, S. Cittolin, R.T. D'Agnolo, A. Holzner, R. Kelley, D. Klein, J. Letts, I. Macneill, D. Olivito, S. Padhi, C. Palmer, M. Pieri, M. Sani, V. Sharma, S. Simon, M. Tadel, Y. Tu, A. Vartak, C. Welke, F. Würthwein, A. Yagil, G. Zevi Della Porta

University of California, Santa Barbara, Santa Barbara, U.S.A.
D. Barge, J. Bradmiller-Feld, C. Campagnari, T. Danielson, A. Dishaw, V. Dutta, K. Flowers, M. Franco Sevilla, P. Geffert, C. George, F. Golf, L. Gouskos, J. Incandela, C. Justus, N. Mccoll, S.D. Mullin, J. Richman, D. Stuart, W. To, C. West, J. Yoo

California Institute of Technology, Pasadena, U.S.A.
A. Apresyan, A. Bornheim, J. Bunn, Y. Chen, J. Duarte, A. Mott, H.B. Newman, C. Pena, M. Pierini, M. Spiropulu, J.R. Vlimant, R. Wilkinson, S. Xie, R.Y. Zhu

Carnegie Mellon University, Pittsburgh, U.S.A.
V. Azzolini, A. Calamba, B. Carlson, T. Ferguson, Y. Iiyama, M. Paulini, J. Russ, H. Vogel, I. Vorobiev

University of Colorado at Boulder, Boulder, U.S.A.
J.P. Cumalat, W.T. Ford, A. Gaz, M. Krohn, E. Luiggi Lopez, U. Nauenberg, J.G. Smith, K. Stenson, S.R. Wagner

Cornell University, Ithaca, U.S.A.
J. Alexander, A. Chatterjee, J. Chaves, J. Chu, S. Dittmer, N. Eggert, N. Mirman, G. Nicolas Kaufman, J.R. Patterson, A. Ryd, E. Salvati, L. Skinnari, W. Sun, W.D. Teo, J. Thom, J. Thompson, J. Tucker, Y. Weng, L. Winstrom, P. Wittich

Fairfield University, Fairfield, U.S.A.
D. Winn

Fermi National Accelerator Laboratory, Batavia, U.S.A.
S. Abdullin, M. Albrow, J. Anderson, G. Apollinari, L.A.T. Bauerdick, A. Beretvas, J. Berryhill, P.C. Bhat, G. Bolla, K. Burkett, J.N. Butler, H.W.K. Cheung, F. Chlebana, S. Cihangir, V.D. Elvira, I. Fisk, J. Freeman, E. Gottschalk, L. Gray, D. Green, S. Grünendahl, O. Gutsche, J. Hanlon, D. Hare, R.M. Harris, J. Hirschauer, B. Hooberman, S. Jindariani, M. Johnson, U. Joshi, B. Klima, B. Kreis, S. Kwan[†], J. Linacre, D. Lincoln, R. Lipton, T. Liu, J. Lykken, K. Maeshima, J.M. Marraffino, V.I. Martinez Outschoorn, S. Maruyama, D. Mason, P. McBride, P. Merkel, K. Mishra, S. Mrenna, S. Nahn, C. Newman-Holmes, V. O'Dell, O. Prokofyev, E. Sexton-Kennedy, A. Soha, W.J. Spalding, L. Spiegel, L. Taylor, S. Tkaczyk, N.V. Tran, L. Uplegger, E.W. Vaandering, R. Vidal, A. Whitbeck, J. Whitmore, F. Yang

University of Florida, Gainesville, U.S.A.
D. Acosta, P. Avery, P. Bortignon, D. Bourilkov, M. Carver, D. Curry, S. Das, M. De Gruttola, G.P. Di Giovanni, R.D. Field, M. Fisher, I.K. Furic, J. Hugon, J. Konigsberg, A. Korytov, T. Kypreos, J.F. Low, K. Matchev, H. Mei, P. Milenovic[54], G. Mitselmakher, L. Muniz, A. Rinkevicius, L. Shchutska, M. Snowball, D. Sperka, J. Yelton, M. Zakaria

Florida International University, Miami, U.S.A.
S. Hewamanage, S. Linn, P. Markowitz, G. Martinez, J.L. Rodriguez

Florida State University, Tallahassee, U.S.A.
J.R. Adams, T. Adams, A. Askew, J. Bochenek, B. Diamond, J. Haas, S. Hagopian, V. Hagopian, K.F. Johnson, H. Prosper, V. Veeraraghavan, M. Weinberg

Florida Institute of Technology, Melbourne, U.S.A.
M.M. Baarmand, M. Hohlmann, H. Kalakhety, F. Yumiceva

University of Illinois at Chicago (UIC), Chicago, U.S.A.
M.R. Adams, L. Apanasevich, D. Berry, R.R. Betts, I. Bucinskaite, R. Cavanaugh, O. Evdokimov, L. Gauthier, C.E. Gerber, D.J. Hofman, P. Kurt, C. O'Brien, I.D. Sandoval Gonzalez, C. Silkworth, P. Turner, N. Varelas

The University of Iowa, Iowa City, U.S.A.
B. Bilki[55], W. Clarida, K. Dilsiz, M. Haytmyradov, J.-P. Merlo, H. Mermerkaya[56], A. Mestvirishvili, A. Moeller, J. Nachtman, H. Ogul, Y. Onel, F. Ozok[48], A. Penzo, R. Rahmat, S. Sen, P. Tan, E. Tiras, J. Wetzel, K. Yi

Johns Hopkins University, Baltimore, U.S.A.
I. Anderson, B.A. Barnett, B. Blumenfeld, S. Bolognesi, D. Fehling, A.V. Gritsan, P. Maksimovic, C. Martin, M. Swartz, M. Xiao

The University of Kansas, Lawrence, U.S.A.
P. Baringer, A. Bean, G. Benelli, C. Bruner, J. Gray, R.P. Kenny III, D. Majumder, M. Malek, M. Murray, D. Noonan, S. Sanders, J. Sekaric, R. Stringer, Q. Wang, J.S. Wood

Kansas State University, Manhattan, U.S.A.
I. Chakaberia, A. Ivanov, K. Kaadze, S. Khalil, M. Makouski, Y. Maravin, L.K. Saini, N. Skhirtladze, I. Svintradze

Lawrence Livermore National Laboratory, Livermore, U.S.A.
J. Gronberg, D. Lange, F. Rebassoo, D. Wright

University of Maryland, College Park, U.S.A.
A. Baden, A. Belloni, B. Calvert, S.C. Eno, J.A. Gomez, N.J. Hadley, S. Jabeen, R.G. Kellogg, T. Kolberg, Y. Lu, A.C. Mignerey, K. Pedro, A. Skuja, M.B. Tonjes, S.C. Tonwar

Massachusetts Institute of Technology, Cambridge, U.S.A.
A. Apyan, R. Barbieri, K. Bierwagen, W. Busza, I.A. Cali, L. Di Matteo, G. Gomez Ceballos, M. Goncharov, D. Gulhan, M. Klute, Y.S. Lai, Y.-J. Lee, A. Levin, P.D. Luckey, C. Paus, D. Ralph, C. Roland, G. Roland, G.S.F. Stephans, K. Sumorok, D. Velicanu, J. Veverka, B. Wyslouch, M. Yang, M. Zanetti, V. Zhukova

University of Minnesota, Minneapolis, U.S.A.
B. Dahmes, A. Gude, S.C. Kao, K. Klapoetke, Y. Kubota, J. Mans, S. Nourbakhsh, R. Rusack, A. Singovsky, N. Tambe, J. Turkewitz

JHEP06(2015)080

University of Mississippi, Oxford, U.S.A.

J.G. Acosta, S. Oliveros

University of Nebraska-Lincoln, Lincoln, U.S.A.

E. Avdeeva, K. Bloom, S. Bose, D.R. Claes, A. Dominguez, R. Gonzalez Suarez, J. Keller, D. Knowlton, I. Kravchenko, J. Lazo-Flores, F. Meier, F. Ratnikov, G.R. Snow, M. Zvada

State University of New York at Buffalo, Buffalo, U.S.A.

J. Dolen, A. Godshalk, I. Iashvili, A. Kharchilava, A. Kumar, S. Rappoccio

Northeastern University, Boston, U.S.A.

G. Alverson, E. Barberis, D. Baumgartel, M. Chasco, A. Massironi, D.M. Morse, D. Nash, T. Orimoto, D. Trocino, R.-J. Wang, D. Wood, J. Zhang

Northwestern University, Evanston, U.S.A.

K.A. Hahn, A. Kubik, N. Mucia, N. Odell, B. Pollack, A. Pozdnyakov, M. Schmitt, S. Stoynev, K. Sung, M. Velasco, S. Won

University of Notre Dame, Notre Dame, U.S.A.

A. Brinkerhoff, K.M. Chan, A. Drozdetskiy, M. Hildreth, C. Jessop, D.J. Karmgard, N. Kellams, K. Lannon, S. Lynch, N. Marinelli, Y. Musienko[28], T. Pearson, M. Planer, R. Ruchti, G. Smith, N. Valls, M. Wayne, M. Wolf, A. Woodard

The Ohio State University, Columbus, U.S.A.

L. Antonelli, J. Brinson, B. Bylsma, L.S. Durkin, S. Flowers, A. Hart, C. Hill, R. Hughes, K. Kotov, T.Y. Ling, W. Luo, D. Puigh, M. Rodenburg, B.L. Winer, H. Wolfe, H.W. Wulsin

Princeton University, Princeton, U.S.A.

O. Driga, P. Elmer, J. Hardenbrook, P. Hebda, S.A. Koay, P. Lujan, D. Marlow, T. Medvedeva, M. Mooney, J. Olsen, P. Piroué, X. Quan, H. Saka, D. Stickland[2], C. Tully, J.S. Werner, A. Zuranski

University of Puerto Rico, Mayaguez, U.S.A.

E. Brownson, S. Malik, H. Mendez, J.E. Ramirez Vargas

Purdue University, West Lafayette, U.S.A.

V.E. Barnes, D. Benedetti, D. Bortoletto, M. De Mattia, L. Gutay, Z. Hu, M.K. Jha, M. Jones, K. Jung, M. Kress, N. Leonardo, D.H. Miller, N. Neumeister, F. Primavera, B.C. Radburn-Smith, X. Shi, I. Shipsey, D. Silvers, A. Svyatkovskiy, F. Wang, W. Xie, L. Xu, J. Zablocki

Purdue University Calumet, Hammond, U.S.A.

N. Parashar, J. Stupak

Rice University, Houston, U.S.A.

A. Adair, B. Akgun, K.M. Ecklund, F.J.M. Geurts, W. Li, B. Michlin, B.P. Padley, R. Redjimi, J. Roberts, J. Zabel

JHEP06(2015)080

University of Rochester, Rochester, U.S.A.
B. Betchart, A. Bodek, P. de Barbaro, R. Demina, Y. Eshaq, T. Ferbel, M. Galanti, A. Garcia-Bellido, P. Goldenzweig, J. Han, A. Harel, O. Hindrichs, A. Khukhunaishvili, S. Korjenevski, G. Petrillo, D. Vishnevskiy

The Rockefeller University, New York, U.S.A.
R. Ciesielski, L. Demortier, K. Goulianos, C. Mesropian

Rutgers, The State University of New Jersey, Piscataway, U.S.A.
S. Arora, A. Barker, J.P. Chou, C. Contreras-Campana, E. Contreras-Campana, D. Duggan, D. Ferencek, Y. Gershtein, R. Gray, E. Halkiadakis, D. Hidas, S. Kaplan, A. Lath, S. Panwalkar, M. Park, R. Patel, S. Salur, S. Schnetzer, D. Sheffield, S. Somalwar, R. Stone, S. Thomas, P. Thomassen, M. Walker

University of Tennessee, Knoxville, U.S.A.
K. Rose, S. Spanier, A. York

Texas A&M University, College Station, U.S.A.
O. Bouhali[57], A. Castaneda Hernandez, R. Eusebi, W. Flanagan, J. Gilmore, T. Kamon[58], V. Khotilovich, V. Krutelyov, R. Montalvo, I. Osipenkov, Y. Pakhotin, A. Perloff, J. Roe, A. Rose, A. Safonov, I. Suarez, A. Tatarinov, K.A. Ulmer

Texas Tech University, Lubbock, U.S.A.
N. Akchurin, C. Cowden, J. Damgov, C. Dragoiu, P.R. Dudero, J. Faulkner, K. Kovitanggoon, S. Kunori, S.W. Lee, T. Libeiro, I. Volobouev

Vanderbilt University, Nashville, U.S.A.
E. Appelt, A.G. Delannoy, S. Greene, A. Gurrola, W. Johns, C. Maguire, Y. Mao, A. Melo, M. Sharma, P. Sheldon, B. Snook, S. Tuo, J. Velkovska

University of Virginia, Charlottesville, U.S.A.
M.W. Arenton, S. Boutle, B. Cox, B. Francis, J. Goodell, R. Hirosky, A. Ledovskoy, H. Li, C. Lin, C. Neu, E. Wolfe, J. Wood

Wayne State University, Detroit, U.S.A.
C. Clarke, R. Harr, P.E. Karchin, C. Kottachchi Kankanamge Don, P. Lamichhane, J. Sturdy

University of Wisconsin, Madison, U.S.A.
D.A. Belknap, D. Carlsmith, M. Cepeda, S. Dasu, L. Dodd, S. Duric, E. Friis, R. Hall-Wilton, M. Herndon, A. Hervé, P. Klabbers, A. Lanaro, C. Lazaridis, A. Levine, R. Loveless, A. Mohapatra, I. Ojalvo, T. Perry, G.A. Pierro, G. Polese, I. Ross, T. Sarangi, A. Savin, W.H. Smith, D. Taylor, C. Vuosalo, N. Woods

†: Deceased
1: Also at Vienna University of Technology, Vienna, Austria

JHEP06(2015)080

2: Also at CERN, European Organization for Nuclear Research, Geneva, Switzerland
3: Also at Institut Pluridisciplinaire Hubert Curien, Université de Strasbourg, Université de Haute Alsace Mulhouse, CNRS/IN2P3, Strasbourg, France
4: Also at National Institute of Chemical Physics and Biophysics, Tallinn, Estonia
5: Also at Skobeltsyn Institute of Nuclear Physics, Lomonosov Moscow State University, Moscow, Russia
6: Also at Universidade Estadual de Campinas, Campinas, Brazil
7: Also at Laboratoire Leprince-Ringuet, Ecole Polytechnique, IN2P3-CNRS, Palaiseau, France
8: Also at Joint Institute for Nuclear Research, Dubna, Russia
9: Also at Suez University, Suez, Egypt
10: Also at Cairo University, Cairo, Egypt
11: Also at Fayoum University, El-Fayoum, Egypt
12: Also at Ain Shams University, Cairo, Egypt
13: Now at British University in Egypt, Cairo, Egypt
14: Also at Université de Haute Alsace, Mulhouse, France
15: Also at Brandenburg University of Technology, Cottbus, Germany
16: Also at Institute of Nuclear Research ATOMKI, Debrecen, Hungary
17: Also at Eötvös Loránd University, Budapest, Hungary
18: Also at University of Debrecen, Debrecen, Hungary
19: Also at University of Visva-Bharati, Santiniketan, India
20: Now at King Abdulaziz University, Jeddah, Saudi Arabia
21: Also at University of Ruhuna, Matara, Sri Lanka
22: Also at Isfahan University of Technology, Isfahan, Iran
23: Also at University of Tehran, Department of Engineering Science, Tehran, Iran
24: Also at Plasma Physics Research Center, Science and Research Branch, Islamic Azad University, Tehran, Iran
25: Also at Università degli Studi di Siena, Siena, Italy
26: Also at Centre National de la Recherche Scientifique (CNRS) - IN2P3, Paris, France
27: Also at Purdue University, West Lafayette, U.S.A.
28: Also at Institute for Nuclear Research, Moscow, Russia
29: Also at St. Petersburg State Polytechnical University, St. Petersburg, Russia
30: Also at National Research Nuclear University 'Moscow Engineering Physics Institute' (MEPhI), Moscow, Russia
31: Also at California Institute of Technology, Pasadena, U.S.A.
32: Also at Faculty of Physics, University of Belgrade, Belgrade, Serbia
33: Also at Facoltà Ingegneria, Università di Roma, Roma, Italy
34: Also at Scuola Normale e Sezione dell'INFN, Pisa, Italy
35: Also at University of Athens, Athens, Greece
36: Also at Paul Scherrer Institut, Villigen, Switzerland
37: Also at Institute for Theoretical and Experimental Physics, Moscow, Russia
38: Also at Albert Einstein Center for Fundamental Physics, Bern, Switzerland
39: Also at Gaziosmanpasa University, Tokat, Turkey
40: Also at Adiyaman University, Adiyaman, Turkey
41: Also at Mersin University, Mersin, Turkey
42: Also at Cag University, Mersin, Turkey
43: Also at Piri Reis University, Istanbul, Turkey
44: Also at Anadolu University, Eskisehir, Turkey
45: Also at Ozyegin University, Istanbul, Turkey

JHEP06(2015)080

46: Also at Izmir Institute of Technology, Izmir, Turkey
47: Also at Necmettin Erbakan University, Konya, Turkey
48: Also at Mimar Sinan University, Istanbul, Istanbul, Turkey
49: Also at Marmara University, Istanbul, Turkey
50: Also at Kafkas University, Kars, Turkey
51: Also at Yildiz Technical University, Istanbul, Turkey
52: Also at Rutherford Appleton Laboratory, Didcot, United Kingdom
53: Also at School of Physics and Astronomy, University of Southampton, Southampton, United Kingdom
54: Also at University of Belgrade, Faculty of Physics and Vinca Institute of Nuclear Sciences, Belgrade, Serbia
55: Also at Argonne National Laboratory, Argonne, U.S.A.
56: Also at Erzincan University, Erzincan, Turkey
57: Also at Texas A&M University at Qatar, Doha, Qatar
58: Also at Kyungpook National University, Daegu, Korea

JHEP06(2015)080